NASA TN D-887

TECHNICAL NOTE

D-887

EFFECTS OF BOATTAILING AND NOZZLE EXTENSION ON THE THRUST-MINUS-DRAG OF A MULTIPLE-JET CONFIGURATION

By William R. Scott

Langley Research Center
Langley Field, Va.

NATIONAL AERONAUTICS AND SPACE ADMINISTRATION

WASHINGTON June 1961

NATIONAL AERONAUTICS AND SPACE ADMINISTRATION

TECHNICAL NOTE D-887

EFFECTS OF BOATTAILING AND NOZZLE EXTENSION ON THE THRUST-MINUS-DRAG OF A MULTIPLE-JET CONFIGURATION

By William R. Scott

SUMMARY

A wind-tunnel investigation of the effects of both boattailing and nozzle extension on the thrust-minus-drag of clustered-jet configurations has been conducted at Mach numbers from 0.60 to 1.40 and jet total-pressure ratios from 3 to 20. Three different boattails were tested: an 8° conical afterbody, a 16° circular-arc afterbody, and a third afterbody having a linear area variation with length. A cylindrical afterbody also was tested for comparison purposes. Extending from these bodies were four circular jet nozzles with a design Mach number of 2.5 which were spaced symmetrically about the body center line.

The results indicated that an 8° conical afterbody provided the highest net thrust efficiency factors of the four models tested when the nozzle exits were at the optimum longitudinal location in each case. The other afterbodies in order of decreasing performance were the 16° circular-arc, the straight-line-area-distribution, and the cylindrical.

INTRODUCTION

Investigations on configurations with both single- and multiple-jet afterbodies have shown that a large base drag force occurs on such afterbodies if they are bluff or cylindrical. Boattailing the afterbody has resulted in substantial reductions in body drag. Extending the nozzles beyond the plane of the base also has been found to be an effective method for reducing jet effects on afterbody drag (ref. 1). In references 2, 3, and 4, various boattail configurations were investigated. Both boattailing and nozzle-extension techniques have also been applied to side-by-side jet exit configurations (refs. 5 and 6).

The investigation reported herein is part of a general program being conducted at the Langley Research Center to study the drag characteristics of multiple-jet configurations. The present investigation was undertaken

to determine the effectiveness of combining nozzle extension with boat-tailing in order to increase the net propulsive force on a clustered-four-jet configuration. An internally mounted strain-gage balance was used to determine the net axial force.

The free-stream Mach number ranged from 0.60 to 1.40. The Reynolds number per foot varied from 3.3×10^6 to 4.4×10^6. The boundary layer was fully turbulent approaching the base, and all tests were made at zero angle of attack. Four different afterbodies were tested, each with four different nozzle lengths. The jet total-pressure ratio was varied from 3 to 20.

SYMBOLS

A	cross-sectional area
C_D	drag coefficient, D/qA_{max}
C_F	thrust coefficient, F/qA_{max}
d	maximum body diameter
D	drag
F	thrust
l	distance from model shoulder to nozzle exit
x	distance from model shoulder to a point on the afterbody
M	Mach number
m	mass flow rate
p	static pressure
p_t	total pressure
$p_{t,j}/p_\infty$	jet total-pressure ratio
q	dynamic pressure, $\frac{1}{2}\rho V^2$
V	velocity
ρ	mass density

γ ratio of specific heats

η efficiency factor, $\frac{C_F - C_D}{C_{F,i}}$

Subscripts:

i ideal, conditions for a fully expanded nozzle

j jet

th theoretical

max maximum

e nozzle exit

∞ free stream

1,2,3,4 lengths of 0.69, 1.16, 2.25, and 3.52 inches, respectively

APPARATUS AND METHODS

Tunnel

The transonic tunnel used in this investigation, shown in figure 1(a), had a $4\frac{1}{2}$- by $4\frac{1}{2}$-inch test section with the top and bottom walls slotted. Air entered the test section through a 30-inch-diameter approach duct at a maximum total pressure of 2 atmospheres and was returned to the atmosphere through a diffuser (area ratio of 1.75). Subsonic Mach number control was achieved by varying the stream total pressure. In order to obtain Mach number control above sonic velocity, suction was applied to the plenum chamber surrounding the test section through an auxiliary pump to reduce the static pressure in the test section. More complete details of the construction of this tunnel and the Mach number distribution along the empty test section can be found in reference 7.

Force Balance

A one-component strain-gage balance was used in this investigation to measure the thrust-minus-drag forces on the models. This force balance is shown in detail in the insert of figure 1(a) and in a larger, simplified sketch in figure 1(b). The balance consisted of two strain

beams which were attached to the internal structure of the balance housing and the model support tube in such a way that loads due to cantilevering of the support tube from the balance did not interact with the balance. Movement of the support tube in the fore-and-aft direction was accomplished with small air leakage by the use of labyrinth seals between the tube and the balance housing. (See fig. 1(b).)

The force balance was enclosed in a cylindrical housing which in turn was supported by struts in the inlet bell of the tunnel. The front (upstream end) of the housing was closed by a hemispherical cap which was pressurized by the leakage of jet air through the front labyrinth seal, and the pressure level was controlled by a valve. (See fig. 1.) The pressure in this cap exerted a force on the end of the support tube which was utilized to oppose the thrust force of the nozzles; thus larger values of absolute thrust could be measured without the sacrifice of strain-gage sensitivity at low pressure. A conical fairing was attached to the rear (downstream end) of the force-balance housing. There was a clearance between the tube and fairing which resulted in a small leakage through the rear labyrinth seal to the tunnel flow.

L
8
6
2

Model Support Tube and Air Supply System

The 1-inch-diameter support tube, which extended from inside the force-balance housing, through the tunnel throat, into the test section, was made up of two parts: a short piece within the housing that was attached to the strain beams, and a longer piece to which the models were attached. The short piece was slotted longitudinally as shown in figure 1 to permit the jet supply air to enter the tube.

The jet supply air entered the balance housing through the top mounting strut and followed the path indicated in the section view of figure 1(b). The jet air was supplied from three 1,000-cubic-foot tanks at atmospheric temperature and a pressure of 310 lb/sq in. A pneumatically operated valve in the air supply pipe outside of the tunnel was utilized to vary the total pressure of the jets.

Models

The 16 afterbody-nozzle configurations are shown in the photographs and sketches of figure 2. Figure 2(b) is a photograph of the four nozzles (design $M = 2.5$ and design $p_{t,j}/p_\infty = 17.1$) showing their different lengths, the three boattailed afterbodies, and the cylindrical afterbody installed in the model support tube. Figure 2(c) is a photograph of the nozzles installed in the afterbodies. Sketches of the models are presented in figure 2(a). In this figure, the location of

the nozzle exit with respect to the afterbody is shown by the small arrows that correspond to the nozzle length. Also given in this figure are the pertinent dimensions of both the afterbodies and the nozzles. The divergence angle of these nozzles was 20°; the divergence was followed by a cylindrical section with a length of one-half of the nozzle exit diameter.

Figure 3 presents a plot of the cross-sectional area of the models as a function of the nondimensionalized distance x/d along the afterbody. The lower curve in each part of the figure represents the area variation of the afterbody alone and the upper curve represents the area variation of the nozzle-afterbody configuration. The dashed line represents the area distribution for the cylindrical afterbody and is included for comparison purposes. The four nozzle lengths are indicated on these plots. The total length of each boattailed afterbody was 3.52 inches as measured from the support-tube shoulder. In the general area distributions of the three boattailed afterbodies, the curve for the straight-line-area-distribution afterbody falls between those for the 8° conical afterbody and the 16° circular-arc afterbody except for a region close to the apex, where the straight-line afterbody has the largest cross-sectional area.

Measurements

The Mach number of the free stream was calculated from the stream total pressure, which was measured in the tunnel approach duct, and the stream static pressure, which was measured in the plenum chamber surrounding the test section. The total pressure of the jet was measured upstream of the nozzle throat.

The total force, which is the sum of the thrust-minus-drag and tare forces, was measured with the strain-gage balance and continuously recorded on pen-trace potentiometers. The significant components of the thrust-minus-drag and the tare forces are indicated on the schematic diagram of the force-balance arrangement presented in figure 1(b). The net thrust-minus-drag force was determined as the difference between the total force readings and the tare forces. The tare forces on the support tube (fig. 1(b)) consisted of: (A) a shear force associated with leakage through the labyrinth seals, (B) the external friction force on the support tube, and (C) the cap-pressure force on the upstream end of the tube. The cap force on the closed, forward end of the support tube was determined from continuously recorded pressure measurements which were obtained by using the cap-pressure pickup tube (item 3, fig. 1(b)). The leakage and friction forces were determined by dynamic calibration tests in which the downstream end of the support tube was sealed as indicated in the sketch of the calibration model in figure 1(b). The conditions

which existed in the balance housing with the models attached to the support tube during the test program were duplicated in the dynamic calibration by running over the entire Mach number range with the internal system pressurized from atmospheric pressure to 310 lb/sq in. and with cap pressures appropriate to the test program. During the dynamic calibration, the additional base force was measured (see fig. 1(b)), and the sum of the leakage and friction tare forces was obtained by subtracting the cap-pressure and base forces from the force indicated by the balance.

Accuracy

The repeatability of these data as determined from plots of the thrust-minus-drag forces corresponded to a maximum error of ±0.10 pound; the maximum error in the faired data curves is estimated to be ±0.05 pound. An error of ±0.05 pound corresponds to the inaccuracies in the net force coefficient and efficiency factor listed in the following table:

M_∞	Error in -	
	$C_F - C_D$	η
0.6	0.020	0.01
.9	.010	.01
1.0	.005	.01
1.2	.005	.01
1.4	.005	.02

RESULTS AND DISCUSSION

Net Thrust Coefficient

The basic force data of this investigation are presented in figures 4 to 7, where the thrust-minus-drag coefficient is plotted as a function of the jet total-pressure ratio for the Mach number range of these tests. Where it was impossible, because of equipment limitations, to obtain the nozzle design pressure ratio, the curves were extrapolated as shown to obtain a value of the thrust-minus-drag coefficient at the design pressure ratio of 17.1. Figure 4 presents thrust-minus-drag coefficients for the 8° conical afterbody with the four different nozzle lengths tested. Similarly, figure 5 presents these data for the 16°

circular-arc afterbody, figure 6 for the boattailed afterbody with the straight-line area distribution, and figure 7 for the cylindrical afterbody.

In all these figures, the thrust-minus-drag coefficient increases linearly as the jet total-pressure ratio is increased. The linear variation can be partly explained from the expression for the nozzle thrust coefficient:

$$C_F = \frac{m_e V_e + (p_e - p_\infty)A_e}{q_\infty A_{max}}$$

which can be written

$$C_F = \frac{\left[\frac{p_{t,j}}{p_\infty}\frac{p_e}{p_{t,j}}\left(1 + \gamma M_e^2\right) - 1\right]\frac{A_e}{A_{max}}}{q_\infty/p_\infty}$$

The preceding expression, which indicates a linear variation of C_F with $p_{t,j}/p_\infty$ (after the nozzle has choked), in combination with the data of figures 4 to 7, which show a linear variation of $C_F - C_D$ with $p_{t,j}/p_\infty$, implies that as the pressure ratio is varied C_D also must have a linear variation within the accuracy of the data. The decrease in the thrust-minus-drag coefficient as the Mach number was increased results from the increase in the dynamic pressure of the free stream, which again can be seen in the preceding equation.

Thrust Efficiency Factor

In order to facilitate the evaluation of the data, the thrust-minus-drag data were converted into an efficiency factor η. This efficiency factor is defined as the measured thrust-minus-drag of the model divided by the thrust of an isentropic nozzle. The following equations were used to calculate η:

$$\eta = \frac{C_F - C_D}{C_{F,i}}$$

and

$$C_{F,i} = \frac{m_{e,th} V_{e,th} + (p_{e,th} - p_\infty)A_{e,th}}{q_\infty A_{max}}$$

where the subscript th refers to theoretical values corresponding to the jet total-pressure ratio. The expression for $C_{F,i}$ can be converted into

$$C_{F,i} = \frac{\gamma M_{e,th}^2 \frac{A_{e,th}}{A_{max}}}{q_\infty/p_\infty}$$

where $M_{e,th}$ and $A_{e,th}$ are functions of $p_{t,j}/p_\infty$.

As all models were tested with the same four nozzles, only the change in net force due to boattailing, nozzle extension, or jet interference is reflected as an increase or decrease in the efficiency factor for a constant value of $p_{t,j}/p_\infty$.

The effect on the efficiency factor of increasing the jet total-pressure ratio is shown in figure 8 for several values of Mach number. The design total-pressure ratio of 17.1 is denoted by the vertical tick in each plot. The curves of figure 8 show that as the jet total-pressure ratio increases the efficiency factor increases at a high rate initially and then tends to level off at the design pressure ratio. The shape of the curves is a property of the internal nozzle thrust, as can be seen from the theoretical curve on the plot for a Mach number of 0.60 in figure 8(a). The theoretical curve is the ratio of the theoretical thrust to the ideal thrust and was computed from the following equation:

$$\eta_{th} = \frac{C_{F,th}}{C_{F,i}} = \frac{\left[\frac{p_{t,j}}{p_\infty}\frac{p_e}{p_{t,j}}\left(1 + \gamma M_e^2\right) - 1\right]\frac{A_e}{A_{e,th}}}{\gamma(M_{e,th})^2}$$

The data curves show the losses in thrust due to off-design operation primarily by their shape, and the difference in the level of efficiency factor between the data curves and the theoretical curves is due to the afterbody drag and losses in nozzle efficiency.

Comparison of Boattail Designs

In figure 8(a), the effect of boattailing can be seen by comparing the four afterbodies at any specific Mach number. It should be remembered that for the cylindrical afterbody the nozzles are extended; thus, this afterbody is better from a drag standpoint than a cylindrical afterbody in which the nozzle exits are flush with the termination of the afterbody. In the boattailed afterbodies the nozzle length of 0.69 inch is not an

extended case. (See fig. 2(a).) The gain in η from the cylindrical afterbody to the lowest-drag boattail is of the order of 5 to 10 percent. For this shortest nozzle length (0.69 inch) the 8° conical afterbody had the highest efficiency over the Mach number range except at a Mach number of 1.40, where for jet total-pressure ratios from 6 to 15 the straight-line-area-distribution afterbody had the highest efficiency.

In a previous investigation of boattail-angle effects (see ref. 8), it was shown that from the drag standpoint an 8° cone was a near optimum configuration over this Mach number range. In figures 8(b) and 8(c), again the 8° conical afterbody with the intermediate nozzle lengths of 1.16 inches and 2.65 inches generally operated more efficiently than the other afterbodies. Thus, with the clustered jet exits this afterbody was still generally better than the others tested. The cylindrical afterbody, from an efficiency standpoint, falls considerably below the other three afterbodies (fig. 8). This low performance is due to the high base drag. In figure 8(d) results are shown for the longest nozzle length of 3.52 inches. There is very little difference here in the efficiency factors for the various boattails because the nozzle exit is located at the downstream tip of the afterbody where the jets have little influence on the boattail.

L
8
6
2

Effect of Nozzle Extension

The effect of nozzle extension is given in figure 9, which presents the efficiency factor η as a function of the nozzle exit location l/d for all test Mach numbers and for values of jet total-pressure ratio of 6, 12, and 18. The parameter l/d is defined as the distance from the shoulder of the afterbody to the nozzle exit divided by the maximum body diameter. Regions of peak values of η are indicated by most of the curves of figure 9, and in many cases η is quite insensitive to the value of l/d in these regions because the peaks of the curves are relatively flat. Small inaccuracies in the value of η used in fairing a given curve would produce a large error in the value of l/d estimated to correspond to the highest value of η because of the limited number of data points available and because of the flat peak regions. Therefore, for a given afterbody and given values of M_∞ and $p_{t,j}/p_\infty$ a curve of figure 9 should be utilized only to determine a range of l/d corresponding to the peak region of η rather than a single optimum value of l/d. The extent of such a range of l/d should be associated with the accuracy of the data and the shape of the individual curve.

The maximum inaccuracy of faired data curves of the efficiency factor η was estimated to vary from 0.01 to 0.02. Accordingly, the average inaccuracies of the faired curves are probably on the order of ± 0.005. The effects of Mach number and jet total-pressure ratio on the range of l/d corresponding to the peak η region are illustrated in

figures 10(a) and 10(b) for the case where ±0.005 was assumed to be the average error. The lower half of the range of l/d is identified by the region between the curve for l/d corresponding to η_{max} and the curve for l/d corresponding to 0.005 less than η_{max} (from fig. 9). The difference between the values of l/d in these two curves is indicative of the accuracy with which the optimum l/d can be determined within the estimated accuracy of η. The dashed portions of the curves represent cases where the region for peak values of η is not well defined in figure 9.

A third curve is presented in figure 10 for which the values of l/d were selected at locations in figure 9 where l/d is less than the indicated optimum by an amount such that η is 0.010 less than the indicated maximum η. A comparison of the curve corresponding to 0.005 less than η_{max} with that corresponding to 0.010 less than η_{max} provides an indication of the reduction in l/d that may be obtained by sacrificing 0.005 in the value of η at the edge of the region for peak values of η.

The curves of figure 10 show that the nozzle extensions required for a maximum efficiency factor for the 8° conical afterbody are shorter than those required by the other afterbodies. The optimum nozzle extensions for the 8° conical afterbody exhibit the least sensitivity to changes in Mach number or jet total-pressure ratio. Specific nozzle-exit locations which would produce negligible losses in efficiency factor over the range of variables presented could be selected in the range of l/d from 1.4 to 1.8. The curves of figure 10(b) for the straight-line-area-distribution afterbody and the cylindrical afterbody exhibit a tendency for the optimum nozzle extensions to increase with increasing Mach number. In most cases the increment of length between the curve for l/d corresponding to 0.005 less than η_{max} and the curve for l/d corresponding to 0.010 less than η_{max} is generally small compared with the increment between the curve for l/d corresponding to η_{max} and that for l/d corresponding to 0.005 less than η_{max}.

Performance With Optimum Nozzle Extension

The maximum values of efficiency factor η were determined from figure 9 and are presented in figure 11 as a function of Mach number for jet total-pressure ratios of 6, 12, and 18 and for the four afterbody designs. Figure 11 permits comparisons of the performance of the four afterbodies for the case where the nozzle extension is always optimum; whereas, figure 8 permitted comparisons for the case where the nozzle extension was a fixed value. The 8° conical afterbody (fig. 11) produced the highest maximum efficiency factors for all combinations of

M_∞ and jet total-pressure ratio. With changes in free-stream Mach number the maximum efficiency factor ranged from 88 percent to 90 percent at a pressure ratio ($p_{t,j}/p_\infty$ of 18) which was slightly over the design value of 17.1. A list of the other afterbodies in order of decreasing performance is the 16° circular-arc, the straight-line-area-distribution, and the cylindrical. The performance of the cylindrical afterbody, in particular, falls off sharply with decreasing values of $p_{t,j}/p_\infty$ or increasing values of M_∞. The cylindrical body produced values of η_{max} which were 0.07 to 0.22 units lower than those for the 8° conical afterbody; the other afterbodies produced values of η_{max} which were 0.01 to 0.04 units lower than those for the 8° conical afterbody.

CONCLUSIONS

The thrust-minus-drag performance of a series of afterbodies with clustered multiple jet exits was determined for a Mach number range from 0.60 to 1.40 and jet total-pressure ratios from 3 to 20. The geometric variables were the shape of the boattailed afterbody and the longitudinal location of the nozzle exits. The ratio of jet exit to body diameter for one jet was equal to 0.36. The tunnel Reynolds number per foot ranged from 3.3×10^6 to 4.4×10^6. The principal conclusions are as follows:

1. The 8° conical afterbody provided the highest net thrust efficiency factors of the four models tested in this investigation when the nozzle exits were at optimum locations for each afterbody. At the design jet total-pressure ratio, the 8° conical afterbody produced maximum efficiency factors which were up to 0.11 higher than those for the cylindrical afterbody and which were up to 0.02 higher than those for the 16° circular-arc and straight-line-area-distribution afterbodies.

2. The optimum nozzle-exit locations of the 8° conical afterbody were the least sensitive to changes in Mach number or jet total-pressure ratio.

Langley Research Center,
National Aeronautics and Space Administration,
Langley Field, Va., March 23, 1961.

REFERENCES

1. Nelson, William J., and Scott, William R.: Jet Effects on the Base Drag of a Cylindrical Afterbody With Extended Nozzles. NACA RM L58A27, 1958.

2. Baughman, L. Eugene: Wind-Tunnel Investigation at Mach 1.9 of Multijet-Missile Base Pressures. NACA RM E54L14, 1955.

3. Leiss, Abraham: Free-Flight Investigation of Effects of Simulated Sonic Turbojet Exhaust on the Drag of Twin-Jet Boattail Bodies at Transonic Speeds. NACA RM L56D30, 1956.

4. Swihart, John M., and Nelson, William J.: Performance of Multiple Jet-Exit Installations. NACA RM L58E01, 1958.

5. Swihart, John M., and Keith, Arvid L., Jr.: An Investigation of Clustered Jet-Exit Arrangements at Supersonic Speeds. NASA MEMO 5-11-59L, 1959.

6. Cubbage, James M., Jr.: Effect of Multiple-Jet Exits on the Base Pressure of a Simple Wing-Body Combination at Mach Numbers of 0.6 to 1.27. NASA TM X-25, 1959.

7. Nelson, William J., and Cubbage, James M., Jr.: Effects of Slot Size and Geometry on the Flow in Rectangular Tunnels at Mach Numbers up to 1.4. NACA RM L53B16, 1953

8. Silhan, Frank V., and Cubbage, James M., Jr.: Drag of Conical and Circular-Arc Boattail Afterbodies at Mach Numbers From 0.6 to 1.3. NACA RM L56K22, 1957.

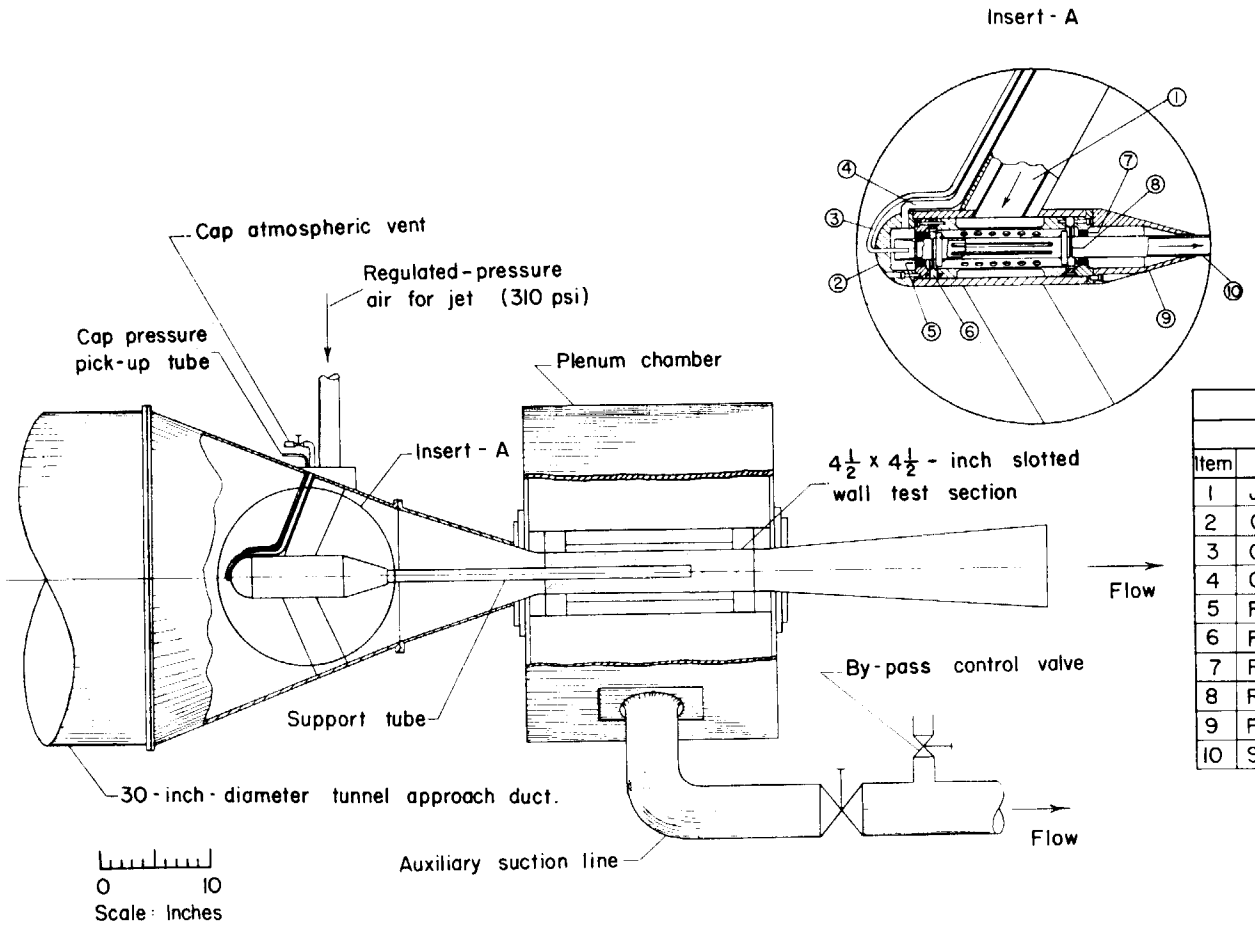

Insert - A	
Force Balance	
Item	Part
1	Jet air supply through strut
2	Cap
3	Cap pressure pick-up tube
4	Cap atmospheric vent tube
5	Front labyrinth seal
6	Front strain beam
7	Rear labyrinth seal
8	Rear strain beam
9	Fairing
10	Support tube

(a) Sketch of setup and detailed insert of force balance.

Figure 1.- Tunnel and force balance.

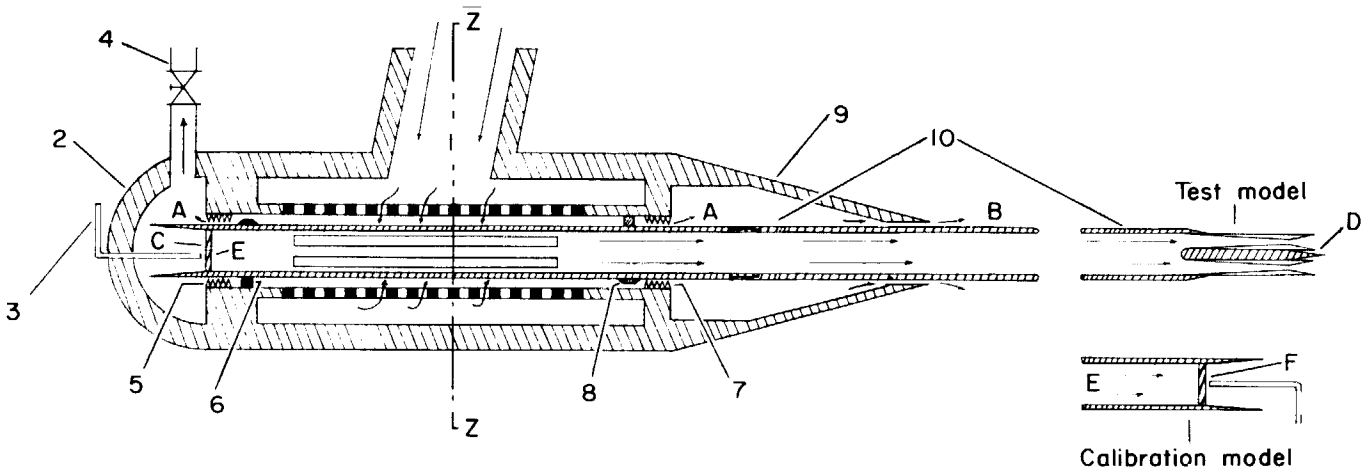

Force Balance	
Item	Part
1	Jet air supply through strut
2	Cap
3	Cap pressure pick-up tube
4	Cap atmospheric vent tube
5	Front labyrinth seal
6	Front strain beam
7	Rear labyrinth seal
8	Rear strain beam
9	Fairing
10	Support tube
11	Perforated housing

Forces			
Tare		Thrust - Drag	
A	Leakage	D	Nozzles and Afterbody
B	Friction	E	Pressure
C	Pressure	F	Base

(b) Simplified sketch of force balance and location of forces.

Figure 1.- Concluded.

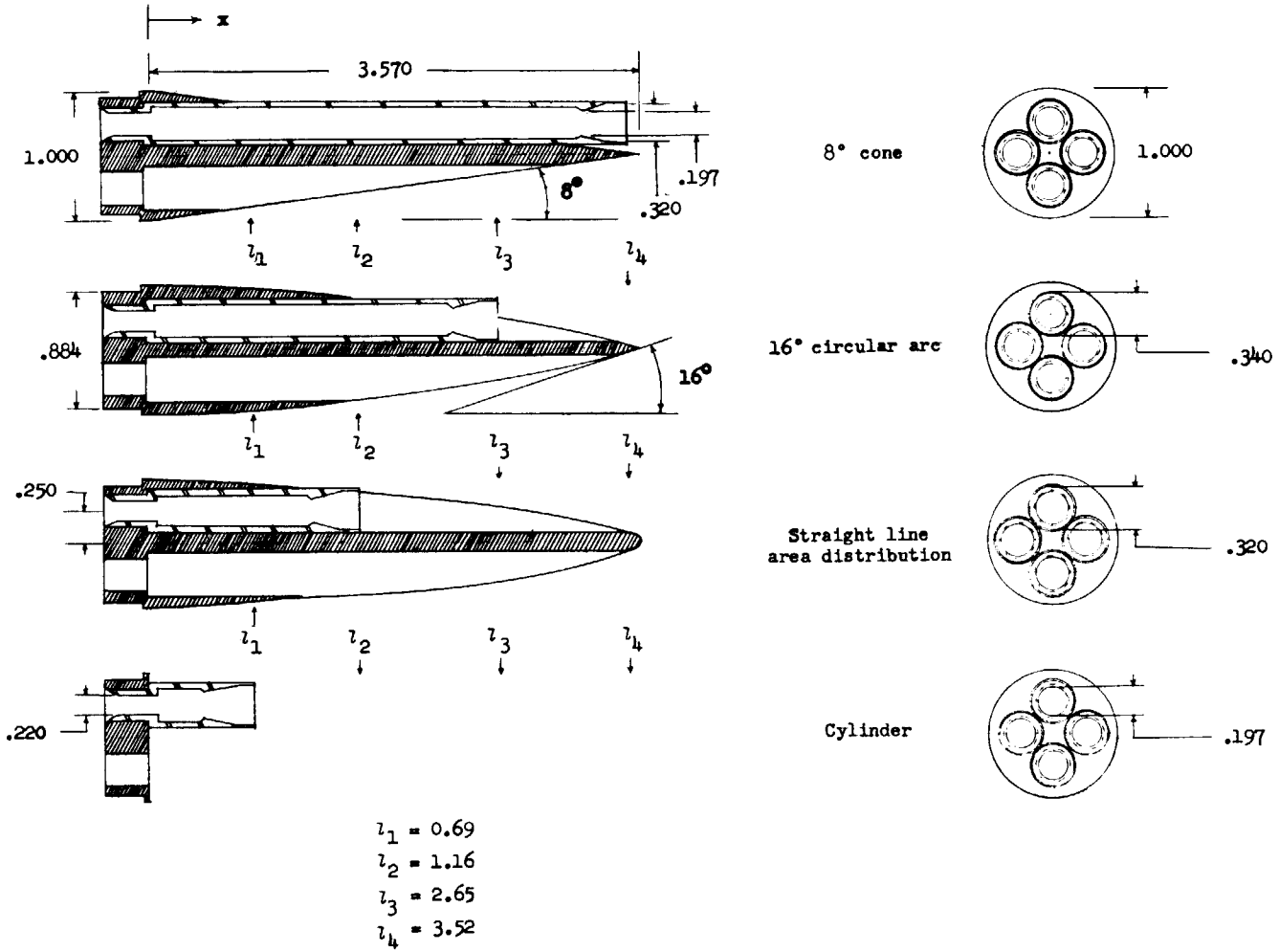

(a) Sketch of afterbodies and nozzles.

Figure 2.- Photographs and sketches of models. All dimensions are in inches.

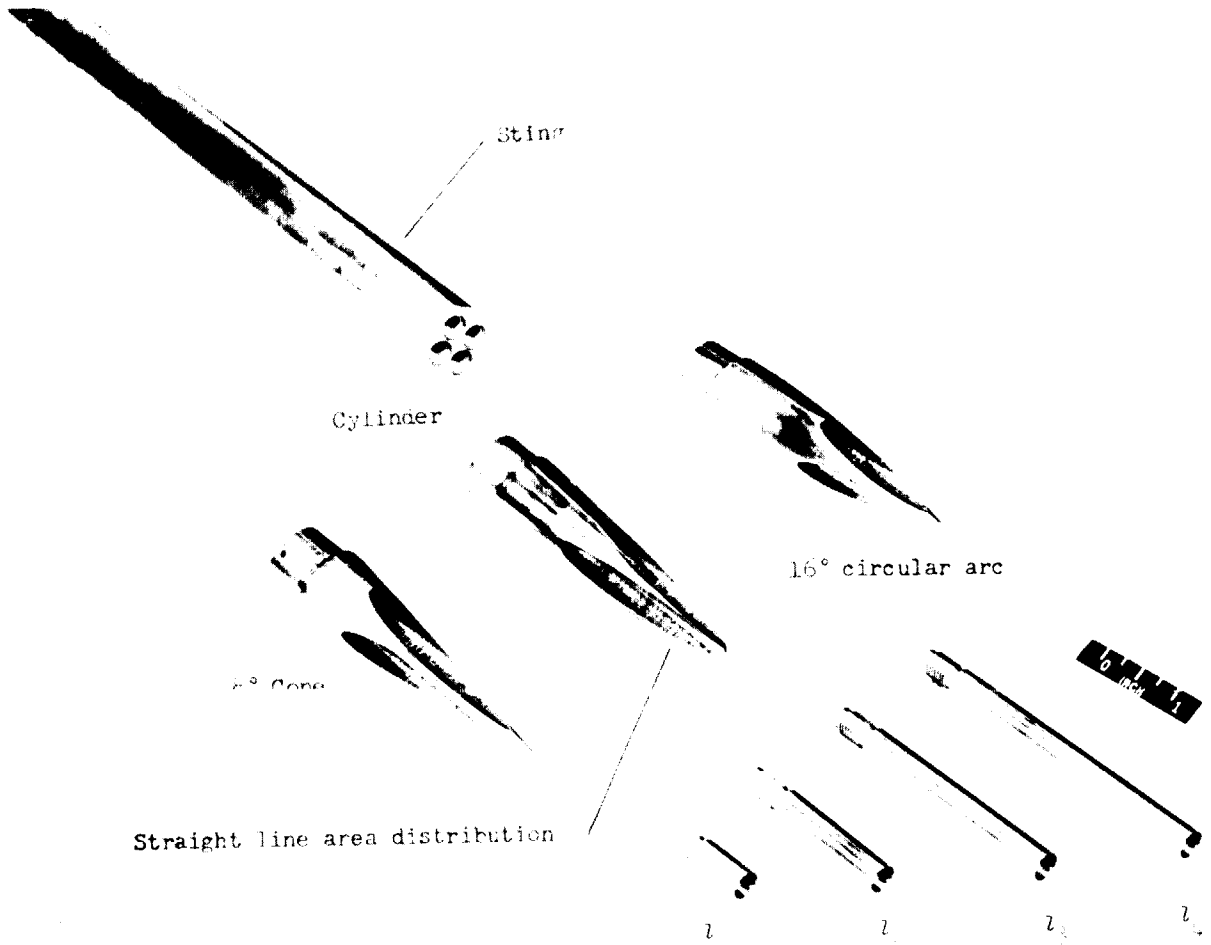

(b) Photograph of sting, afterbodies, and nozzles. L-59-5535

Figure 2.- Continued.

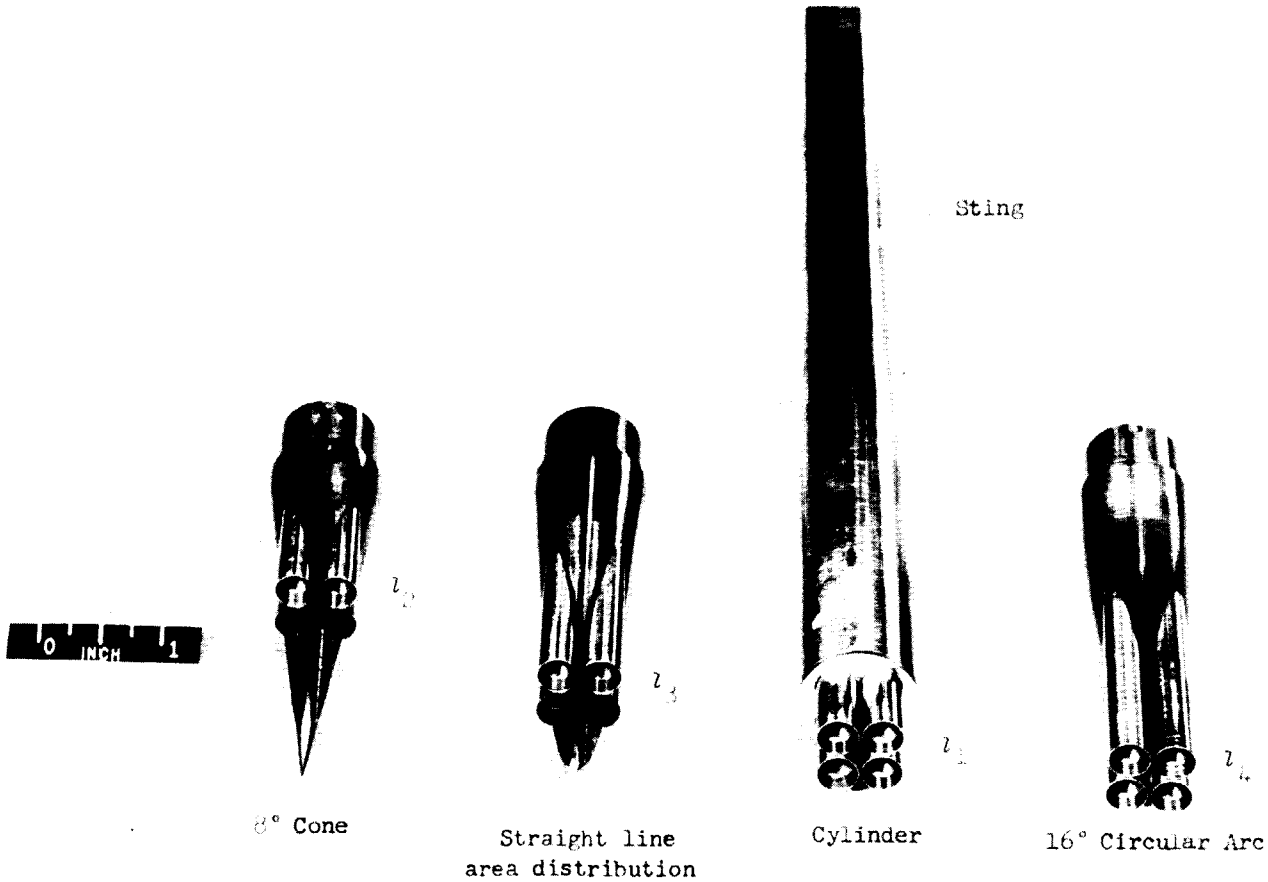

(c) Photograph of afterbodies with nozzles installed. L-59-5536

Figure 2.- Concluded.

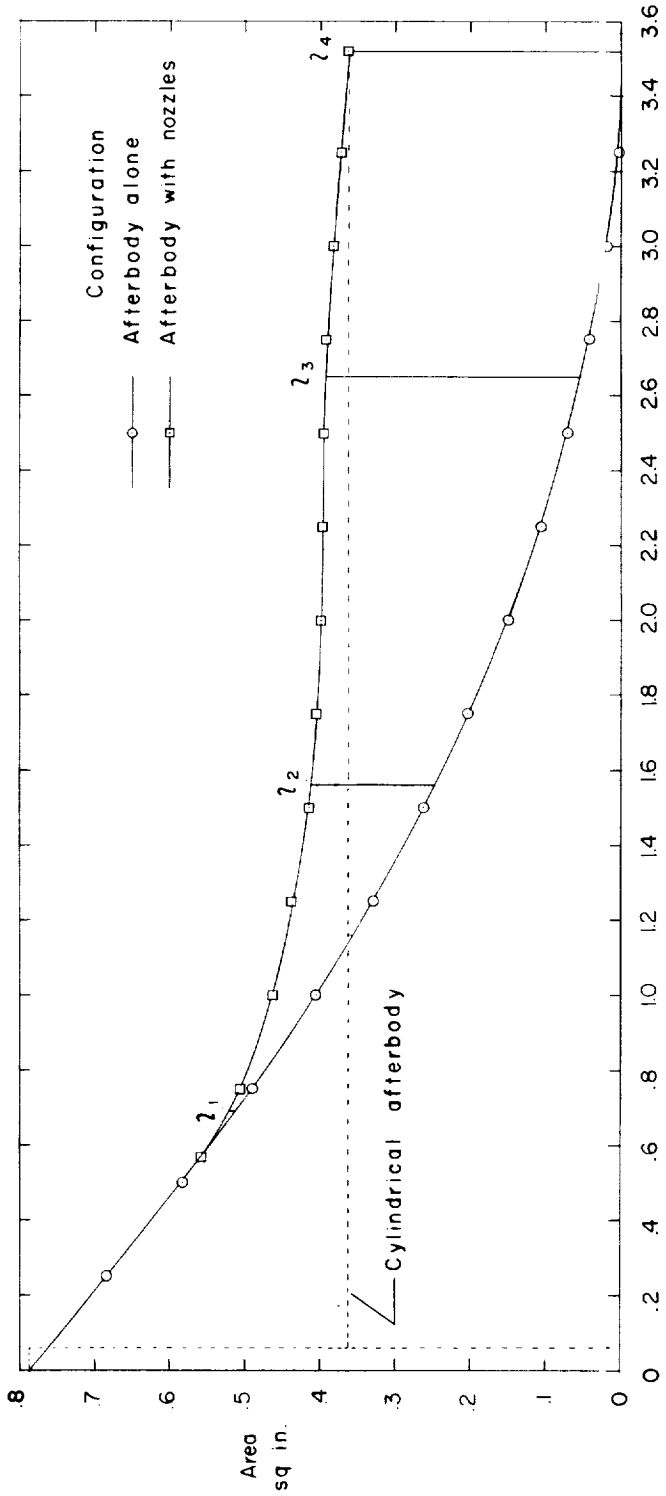

(a) 8° conical afterbody.

Figure 3.- Cross-sectional area of models with nozzle area included.

L-862

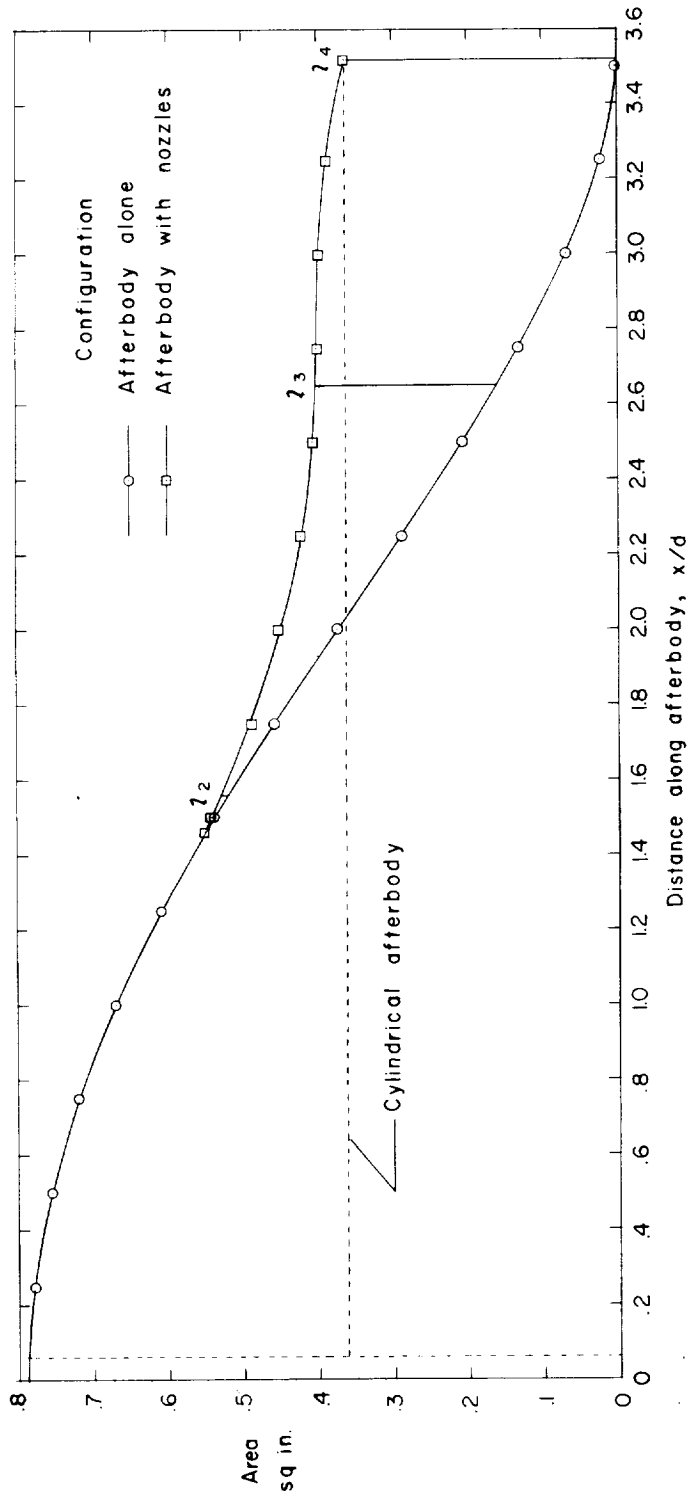

(b) 16° circular-arc afterbody.

Figure 3.- Continued.

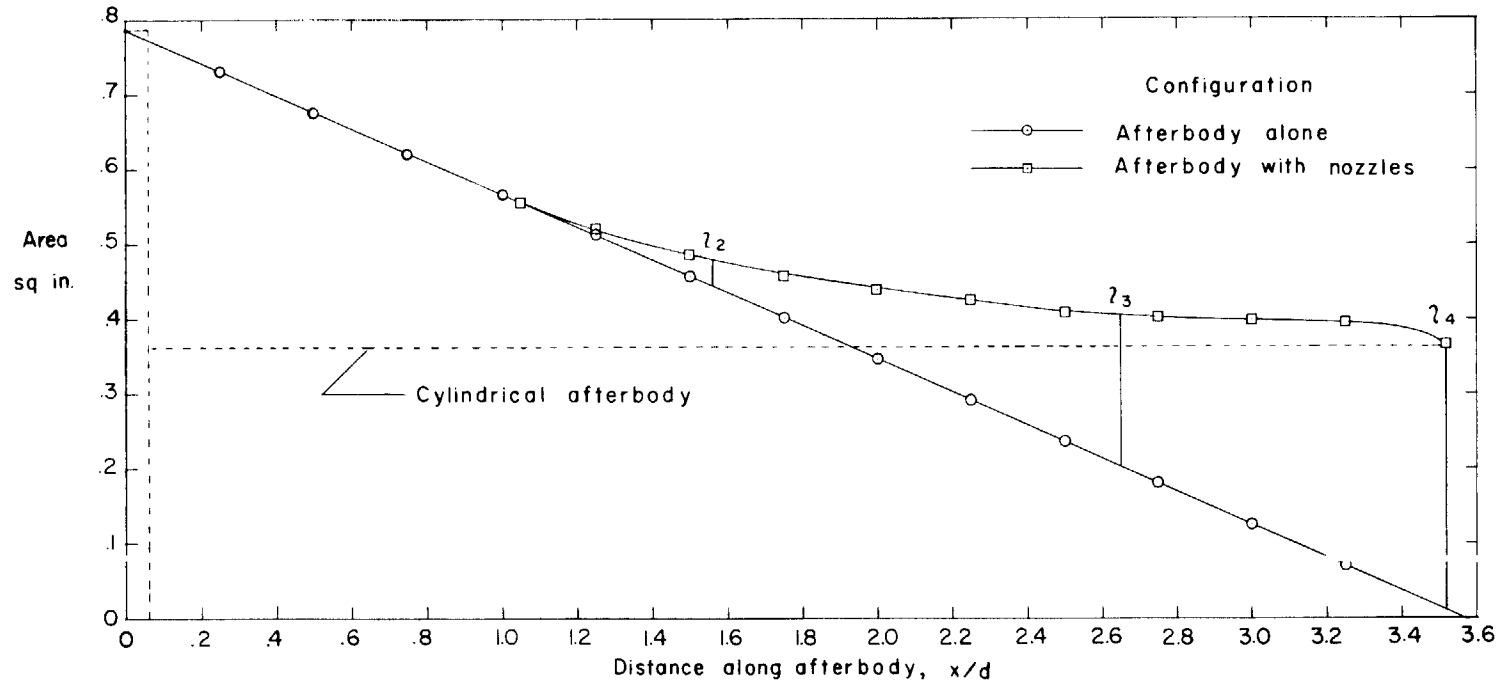

(c) Straight-line-area-distribution afterbody.

Figure 3.- Concluded.

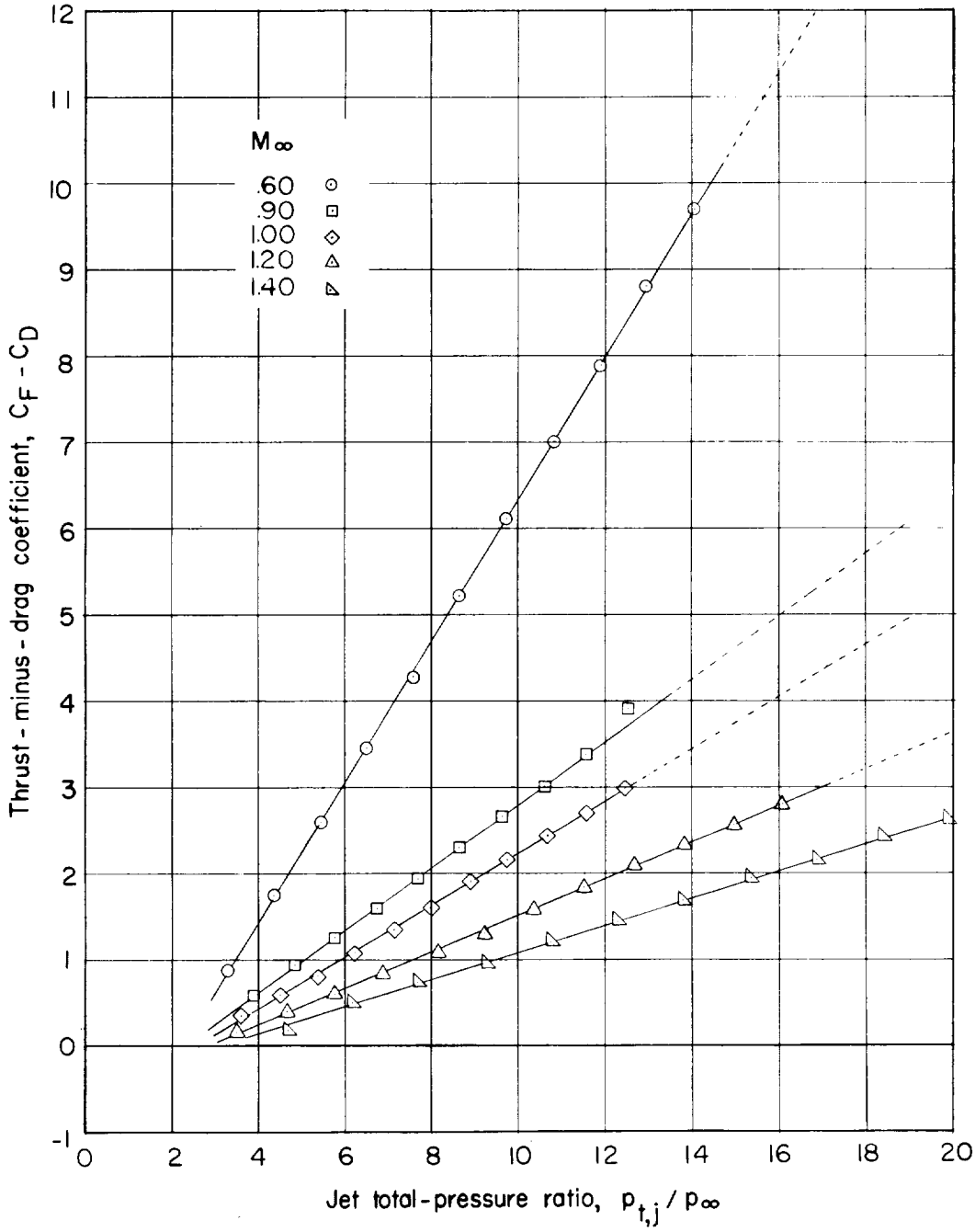

(a) Nozzle length of 0.69 inch.

Figure 4.- Effect of jet total-pressure ratio on measured thrust-minus-drag coefficient on 8° conical afterbody.

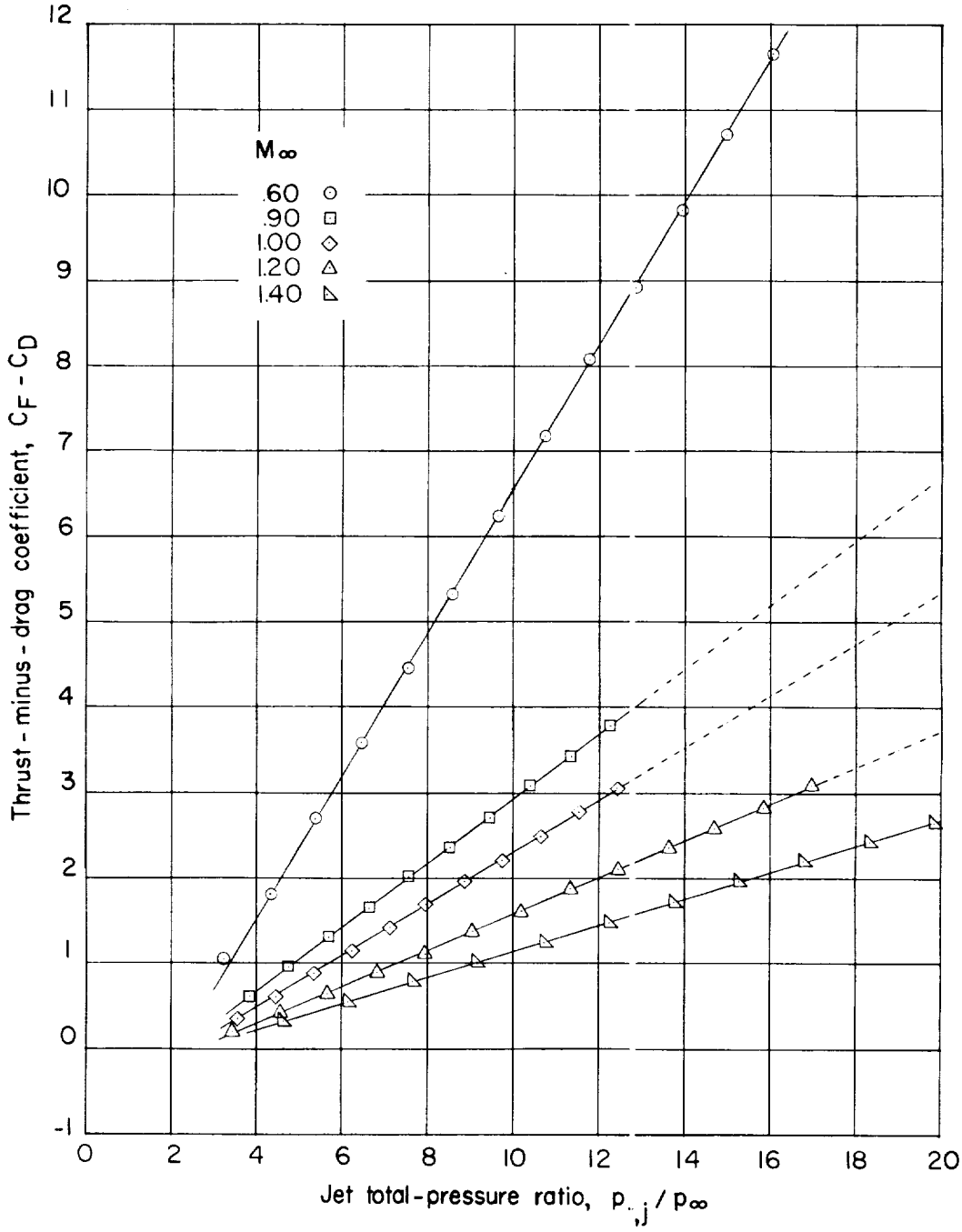

(b) Nozzle length of 1.16 inches.

Figure 4.- Continued.

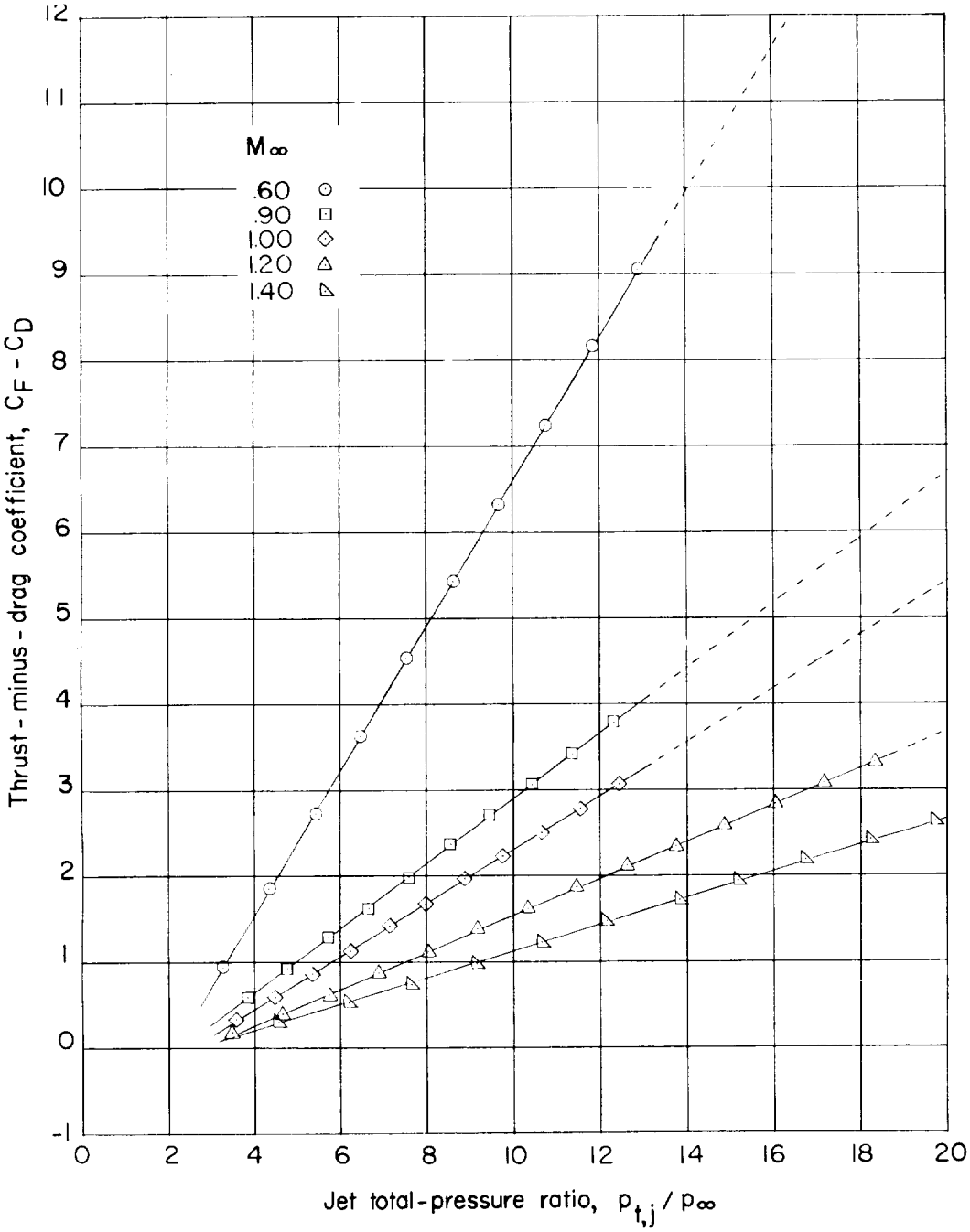

(c) Nozzle length of 2.65 inches.

Figure 4.- Continued.

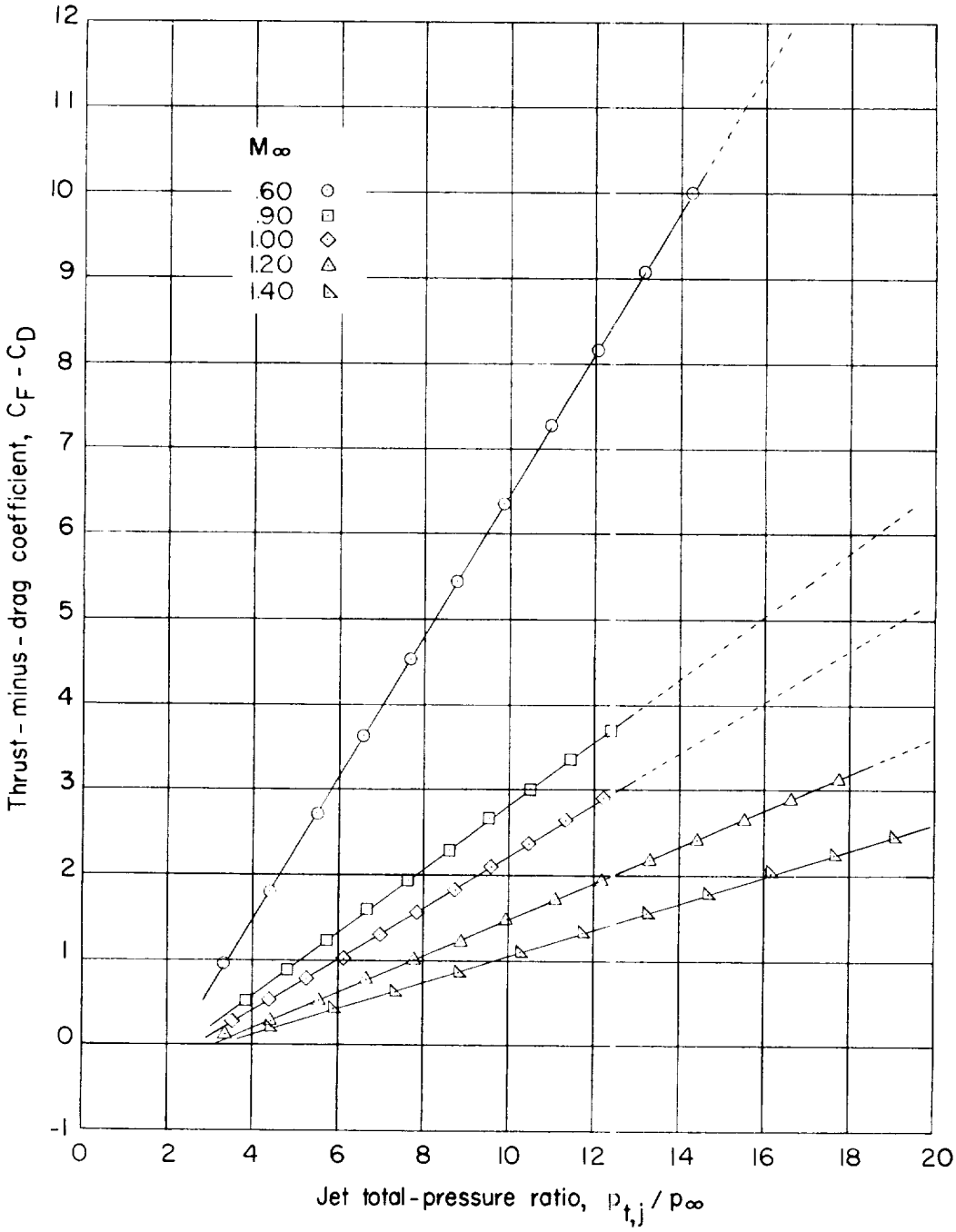

(d) Nozzle length of 3.52 inches.

Figure 4.- Concluded.

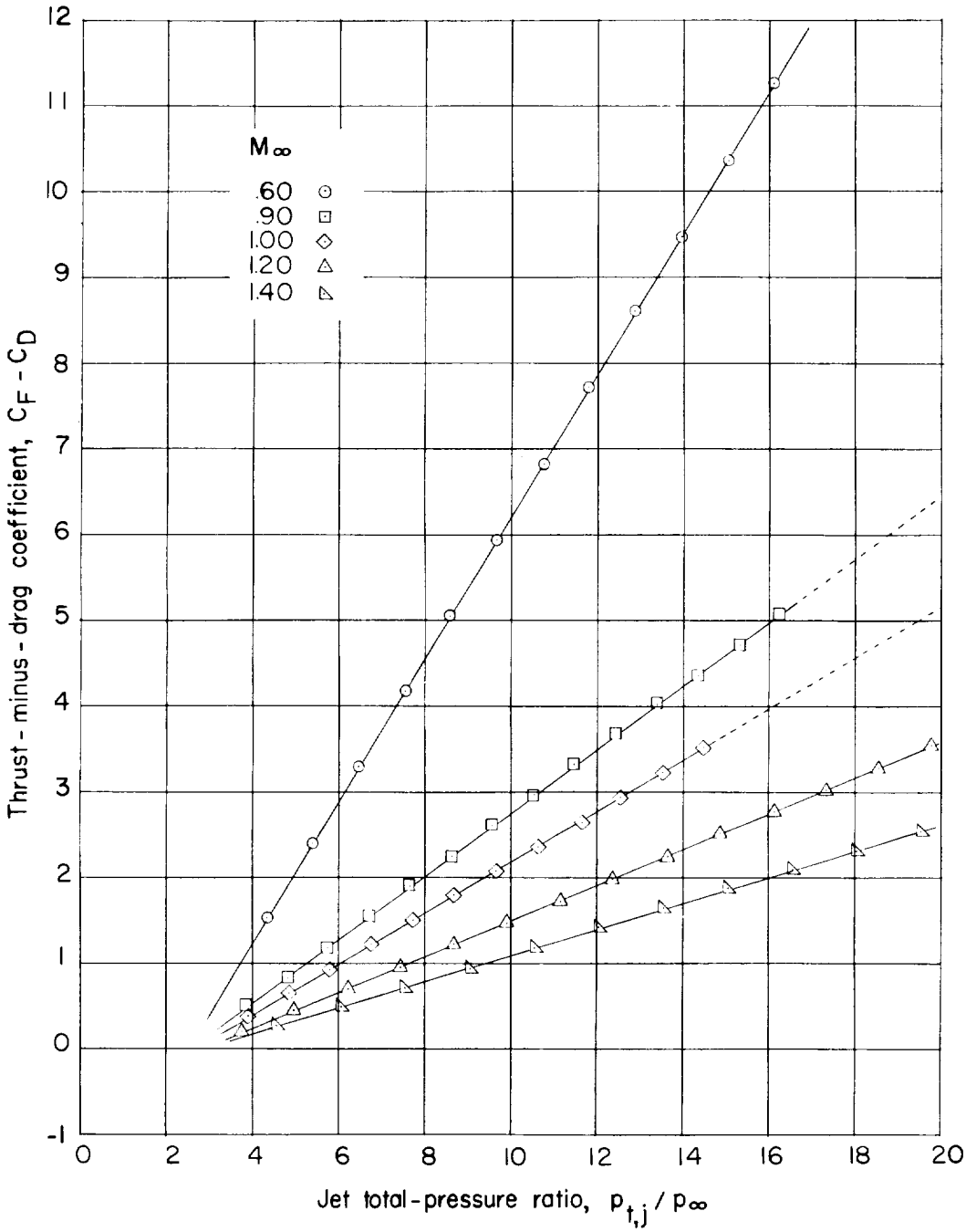

(a) Nozzle length of 0.69 inch.

Figure 5.- Effect of jet total-pressure ratio on measured thrust-minus-drag coefficient on 16° circular-arc afterbody.

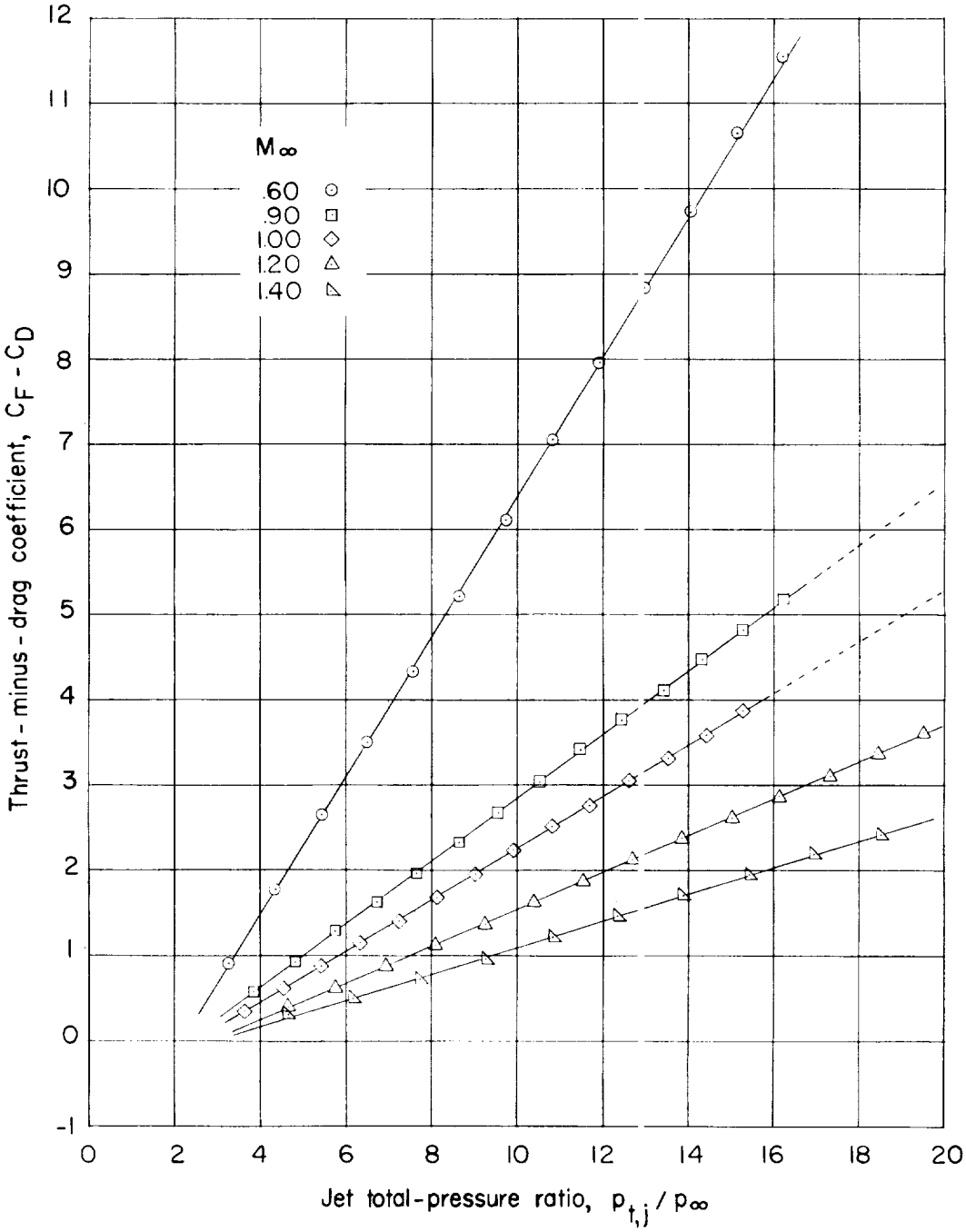

(b) Nozzle length of 1.16 inches.

Figure 5.- Continued.

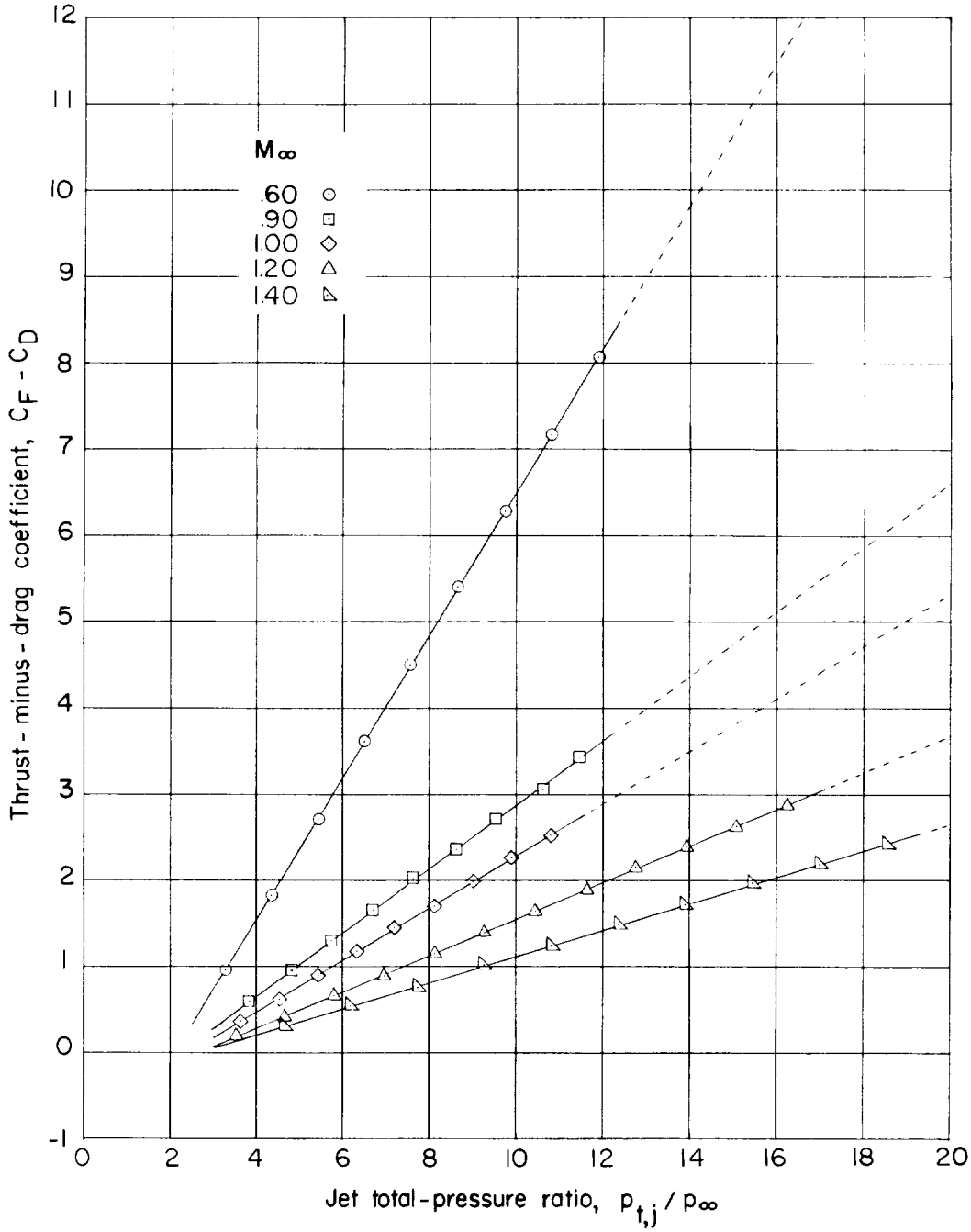

(c) Nozzle length of 2.65 inches.

Figure 5.- Continued.

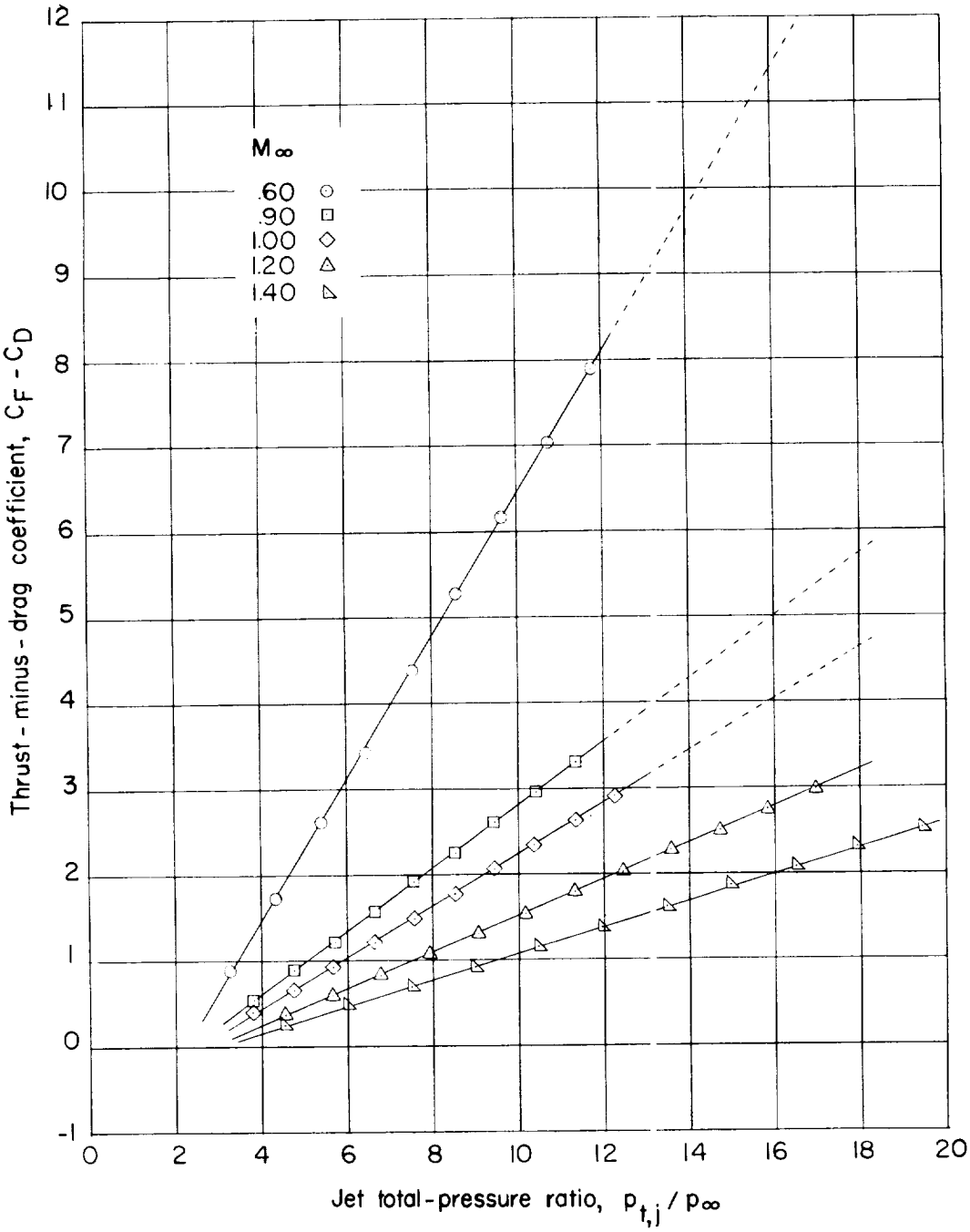

(d) Nozzle length of 3.52 inches.

Figure 5.- Concluded.

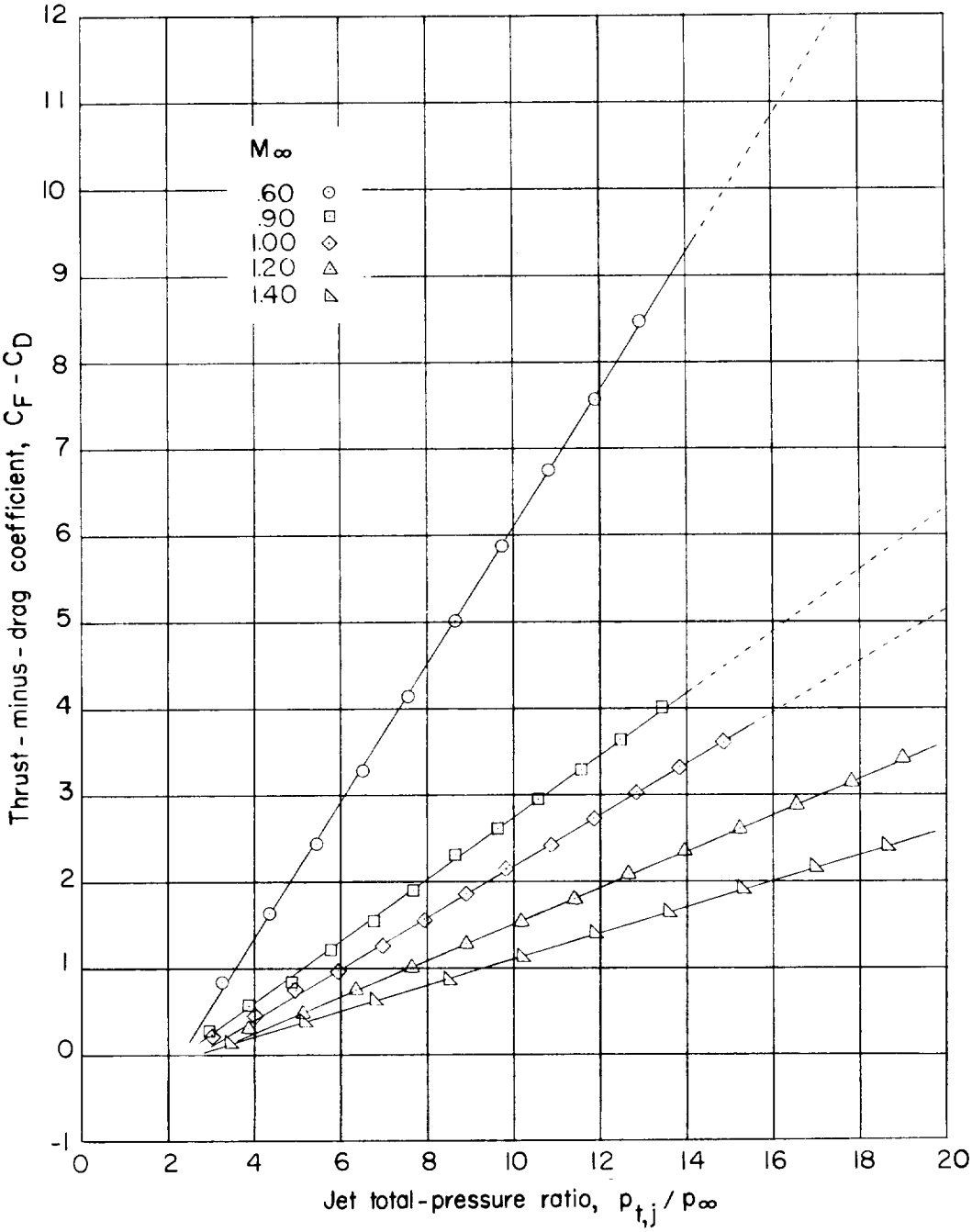

(a) Nozzle length of 0.69 inch.

Figure 6.- Effect of jet total-pressure ratio on measured thrust-minus-drag coefficient on straight-line-area-distribution afterbody.

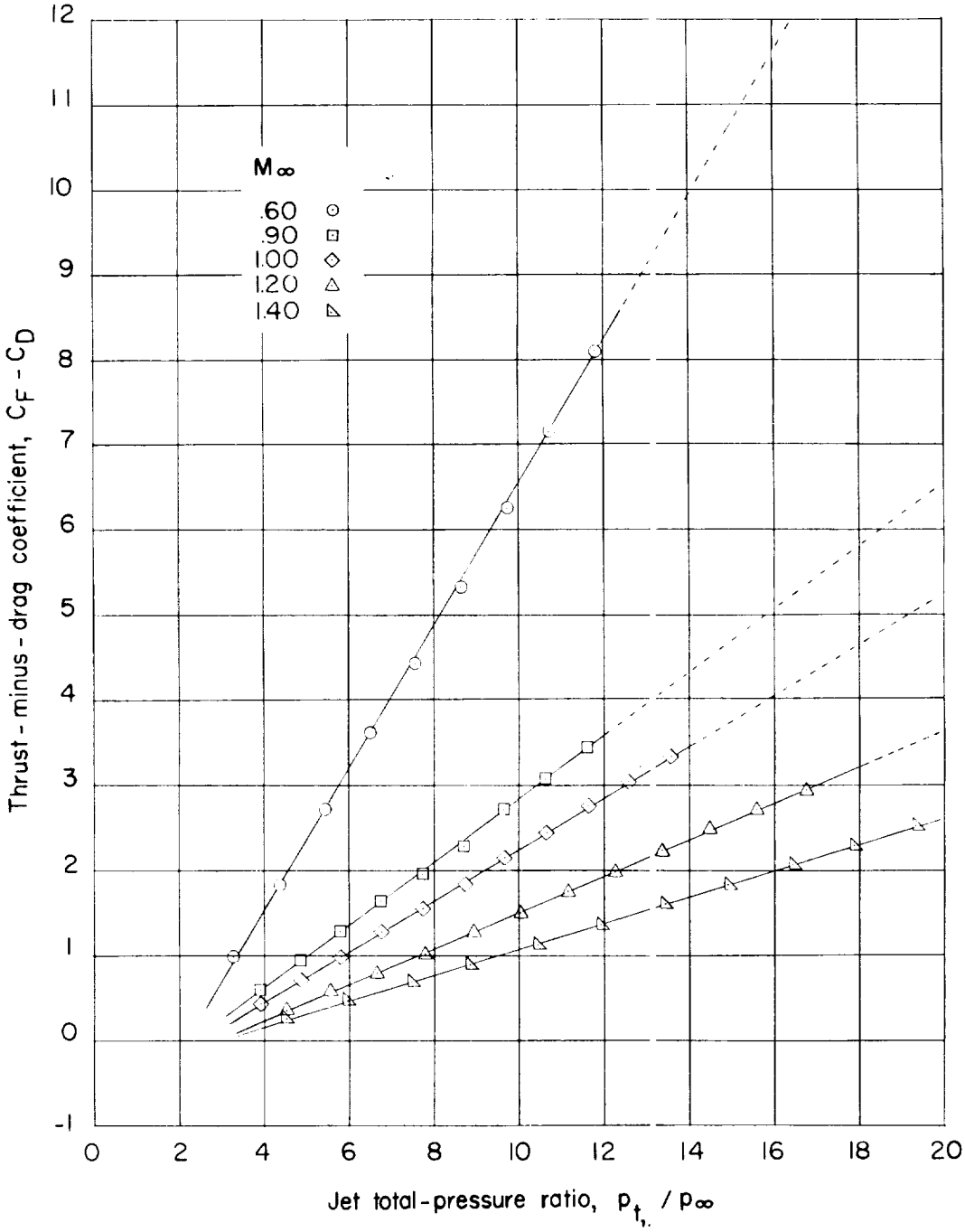

(b) Nozzle length of 1.16 inches.

Figure 6.- Continued.

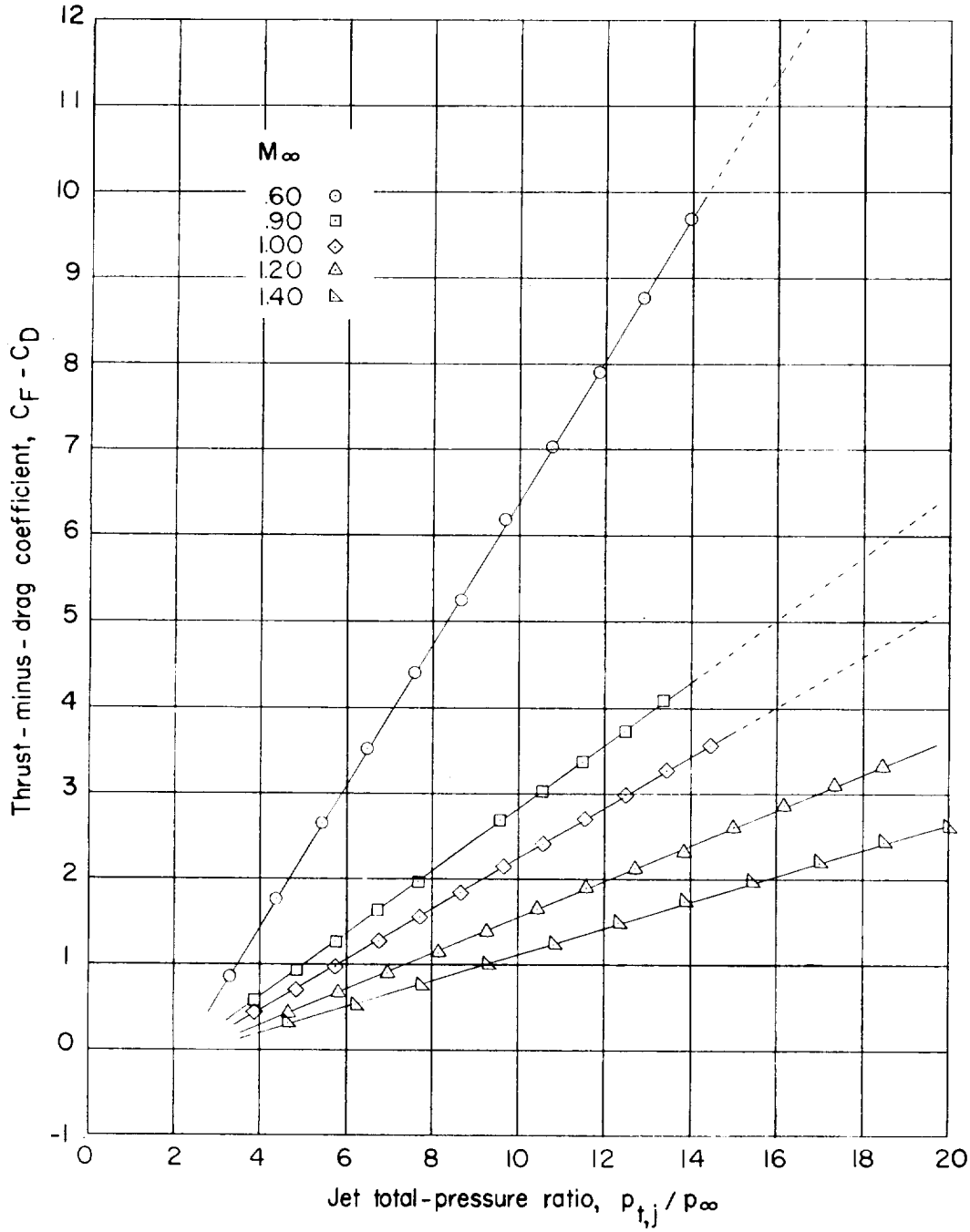

(c) Nozzle length of 2.65 inches.

Figure 6.- Continued.

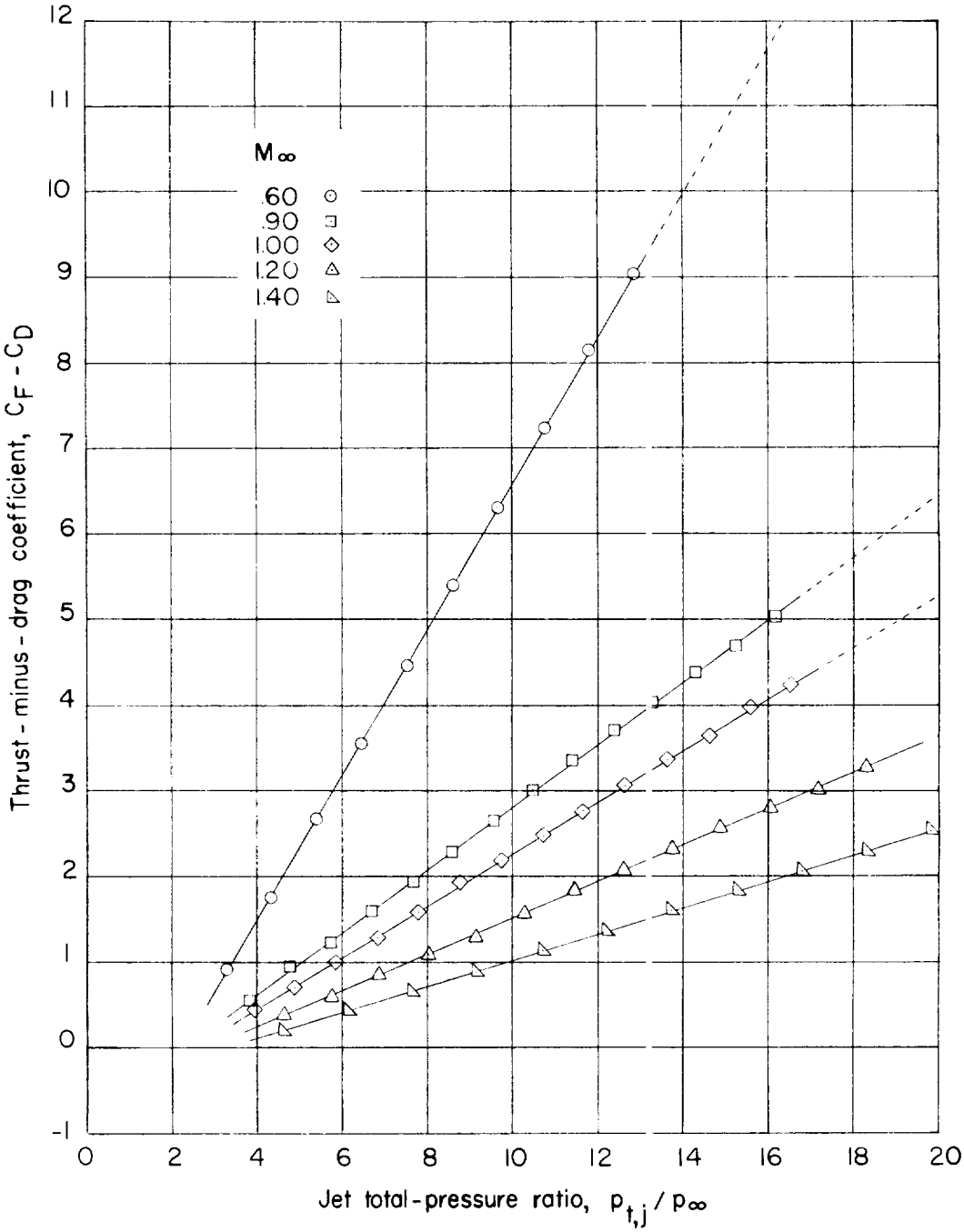

(d) Nozzle length of 3.52 inches.

Figure 6.- Concluded.

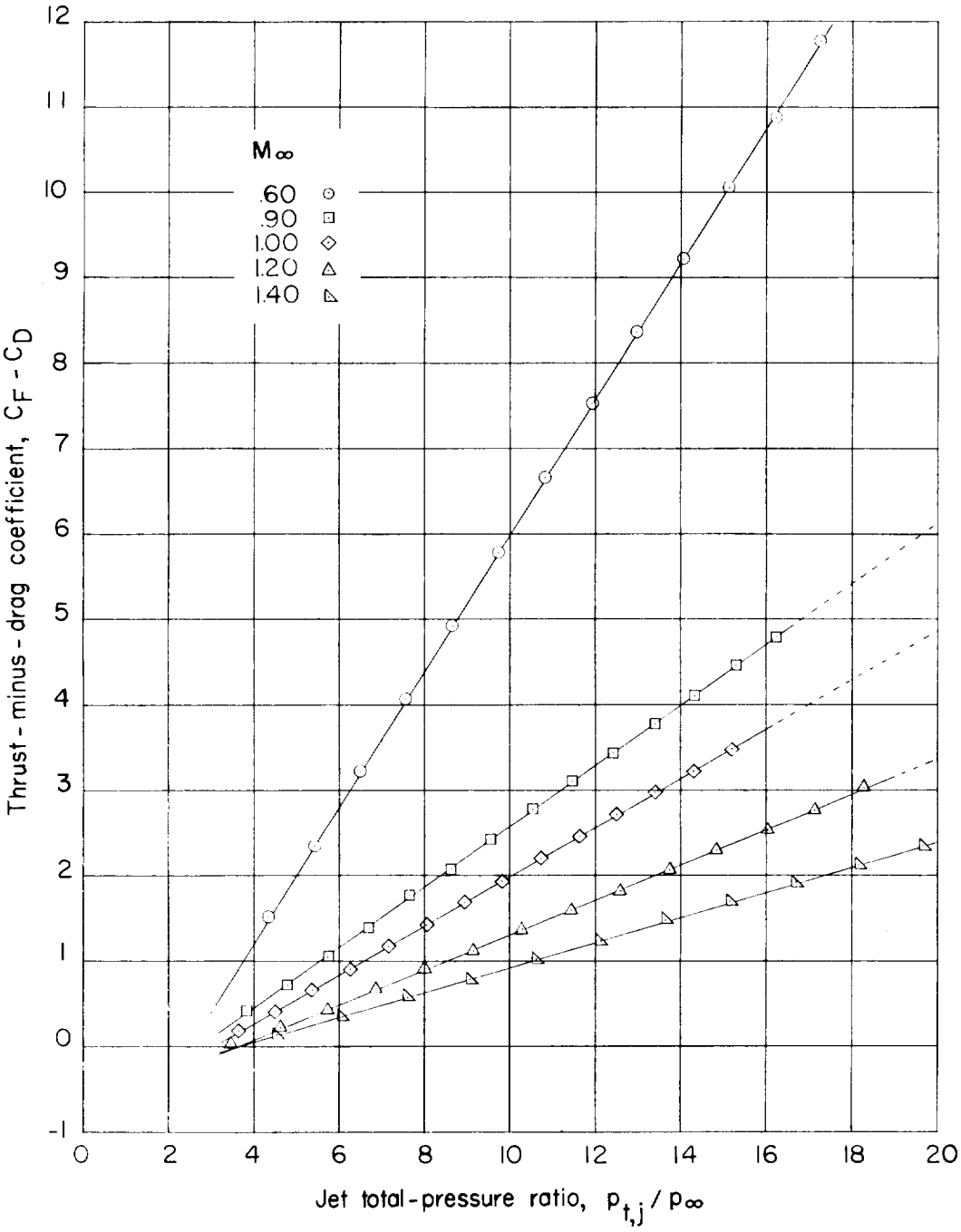

(a) Nozzle length of 0.69 inch.

Figure 7.- Effect of jet total-pressure ratio on measured thrust-minus-drag coefficient on cylindrical afterbody.

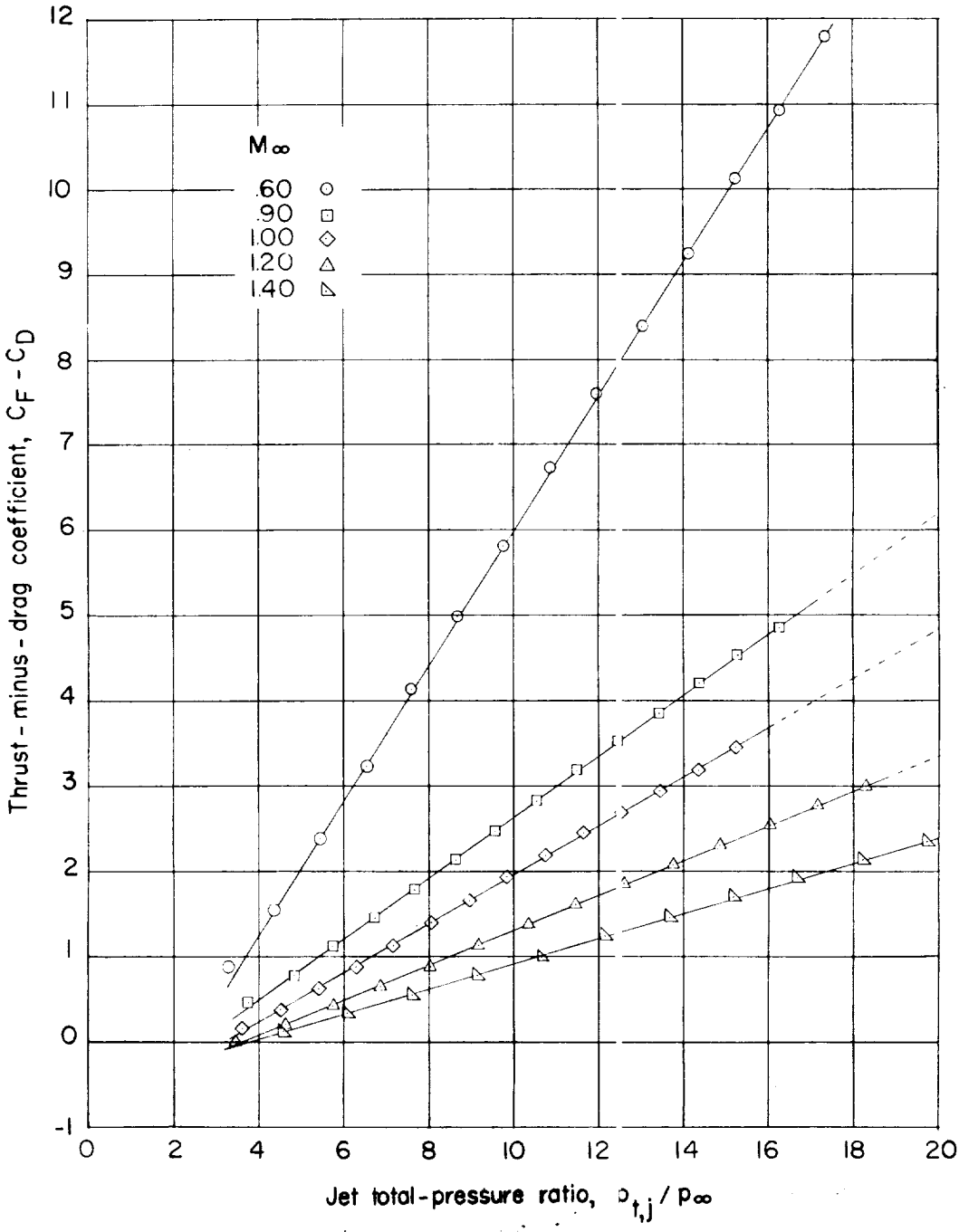

(b) Nozzle length of 1.16 inches.

Figure 7.- Continued.

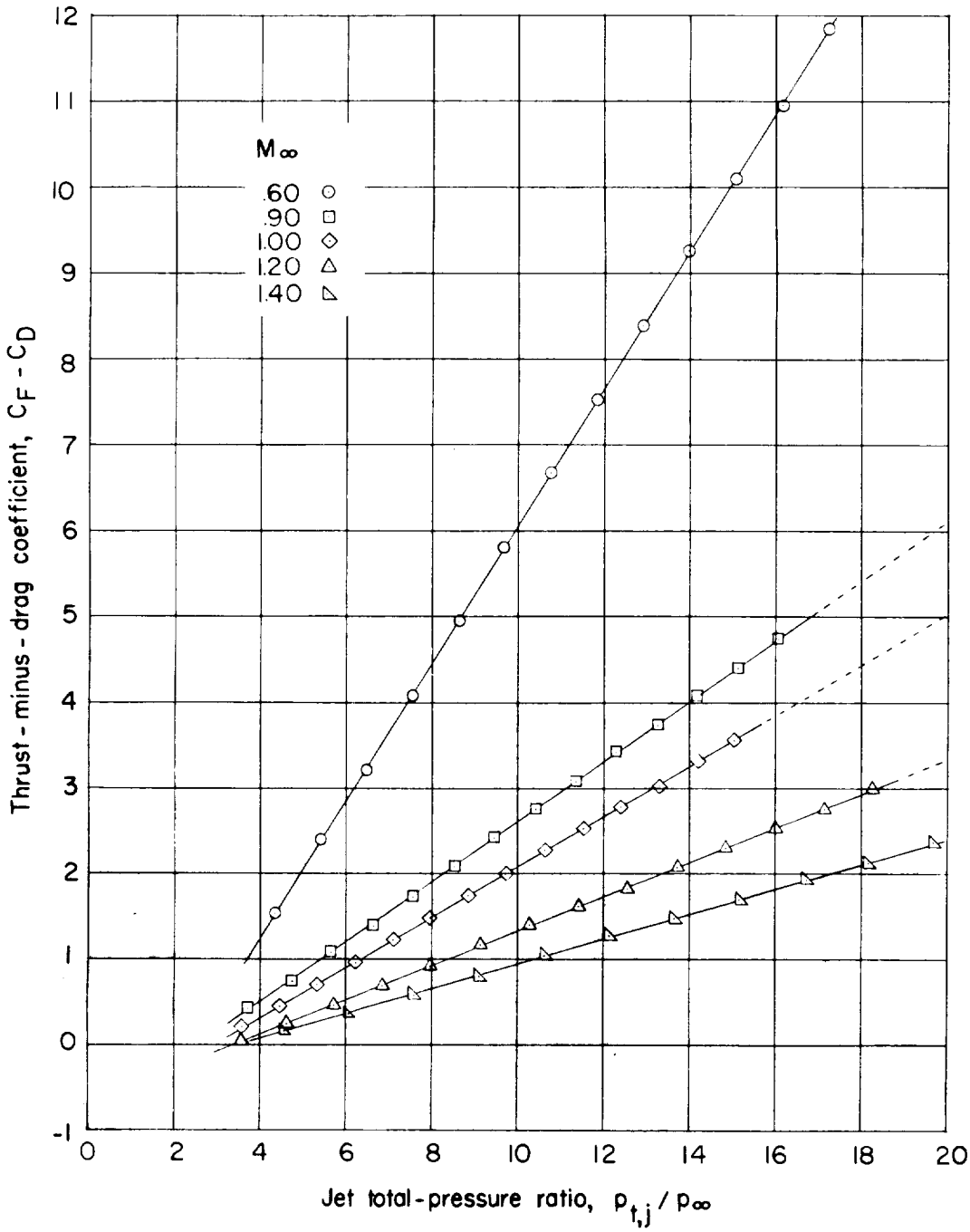

(c) Nozzle length of 2.65 inches.

Figure 7.- Continued.

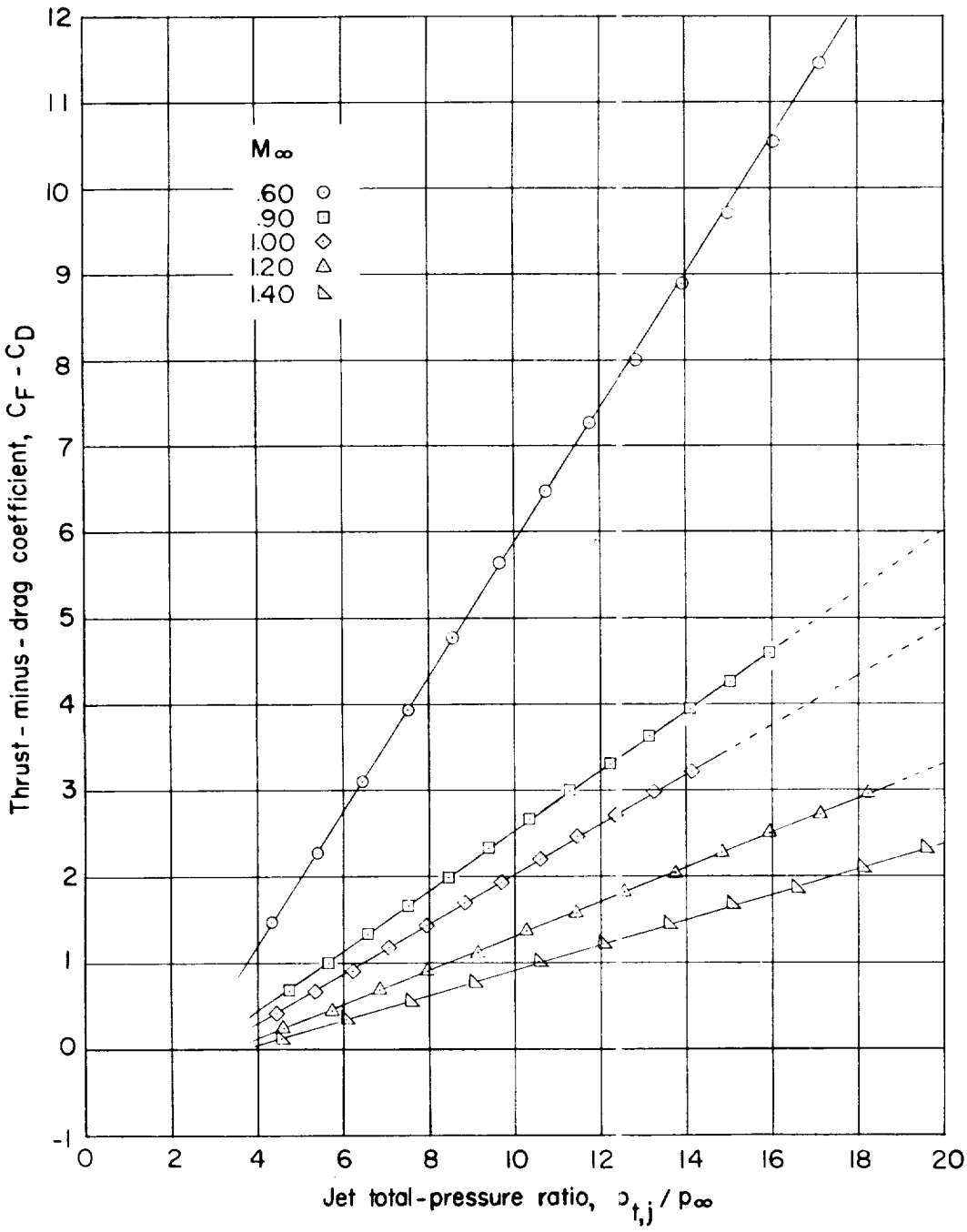

(d) Nozzle length of 3.52 inches.

Figure 7.- Concluded.

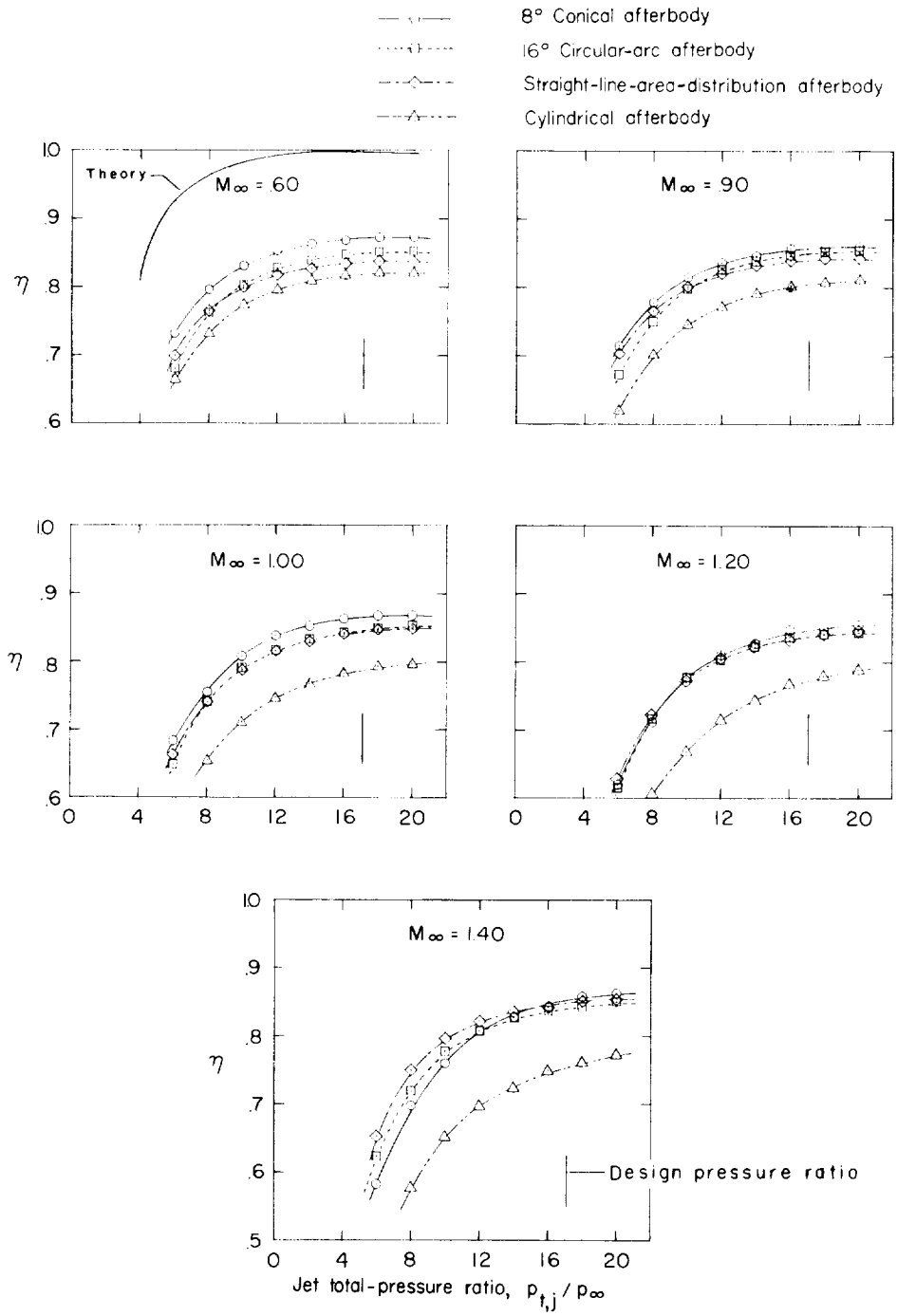

(a) Nozzle length of 0.69 inch.

Figure 8.- Effect of jet total-pressure ratio on the efficiency factor.

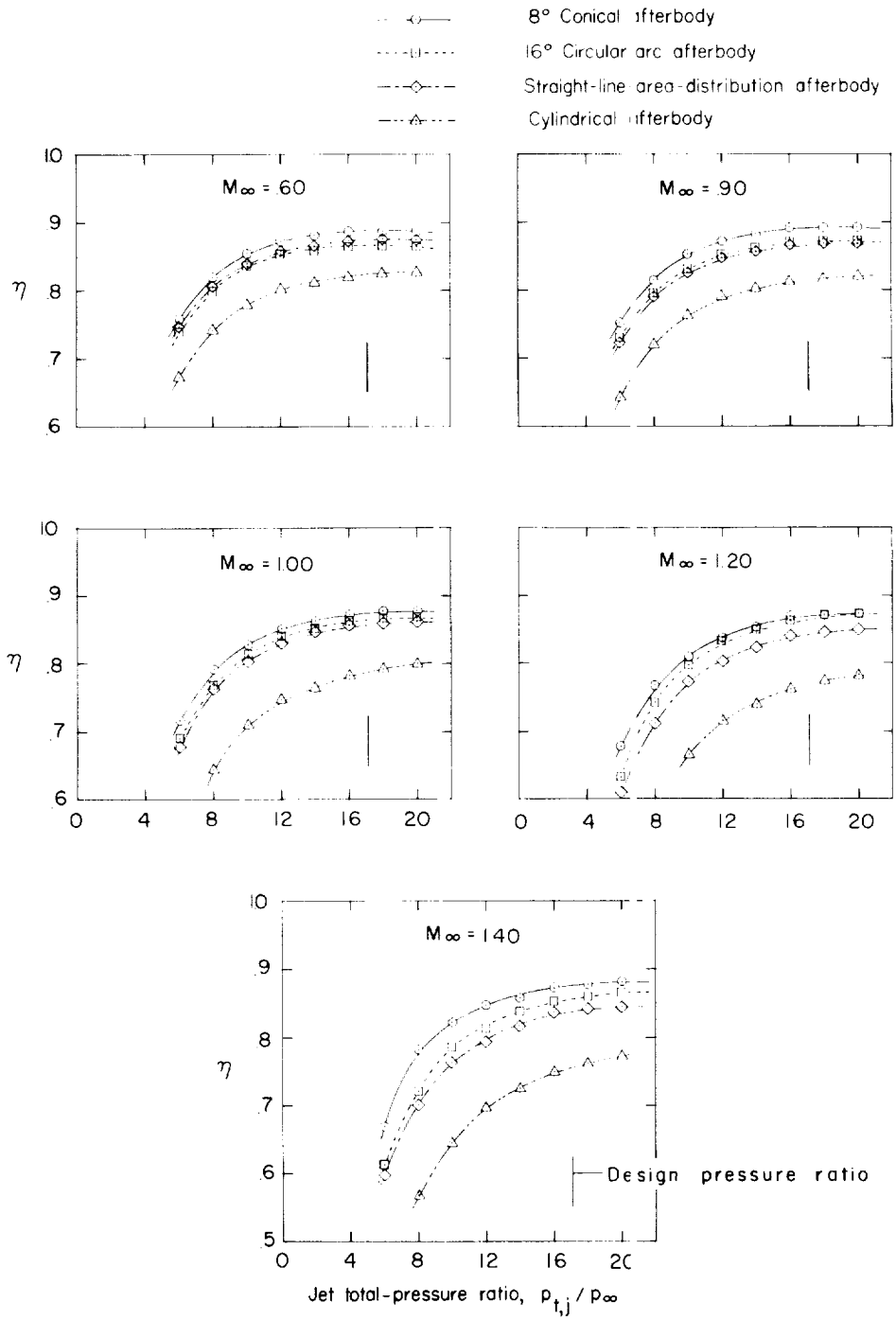

(b) Nozzle length of 1.16 inches.

Figure 8.- Continued.

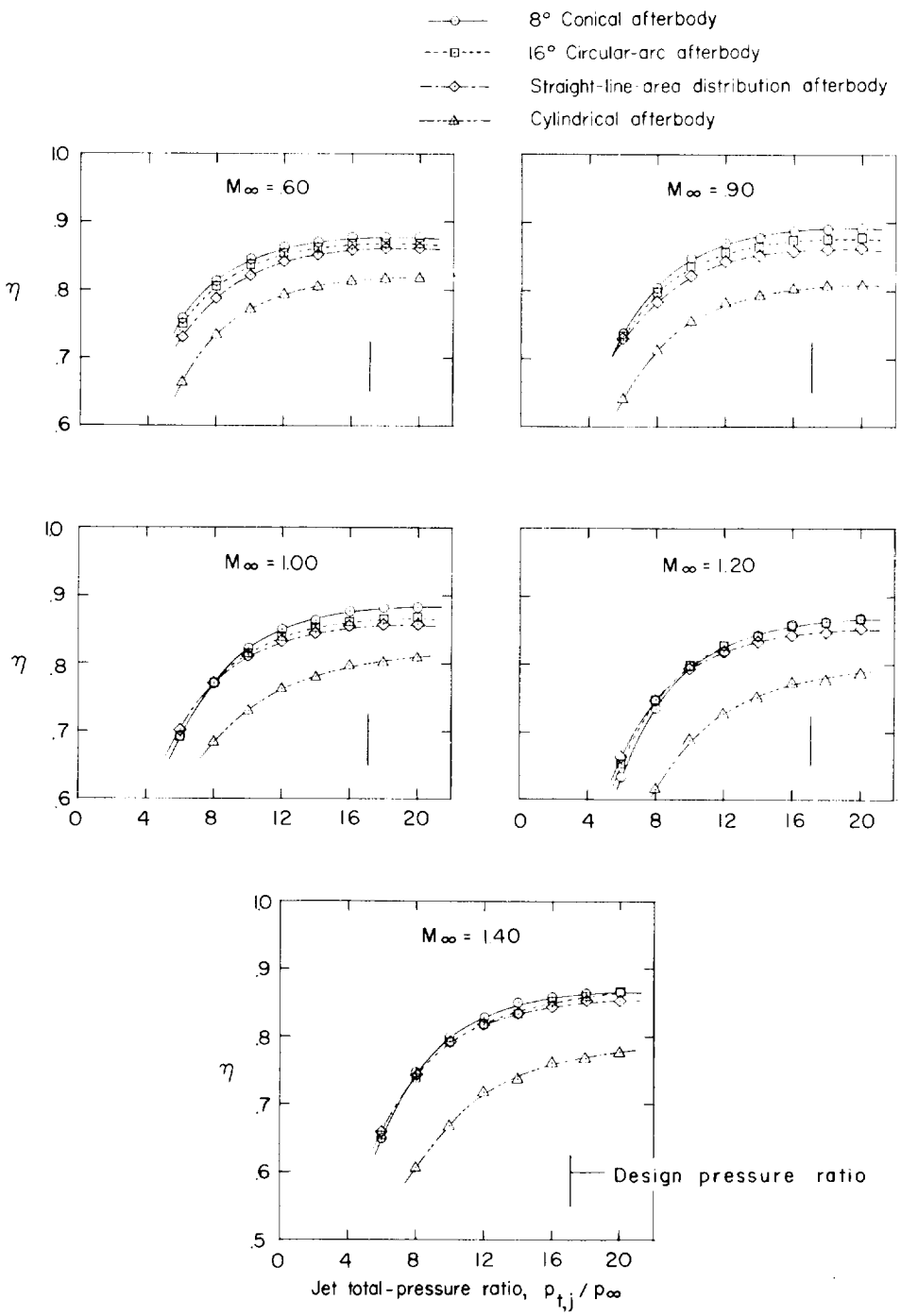

(c) Nozzle length of 2.65 inches.

Figure 8.- Continued.

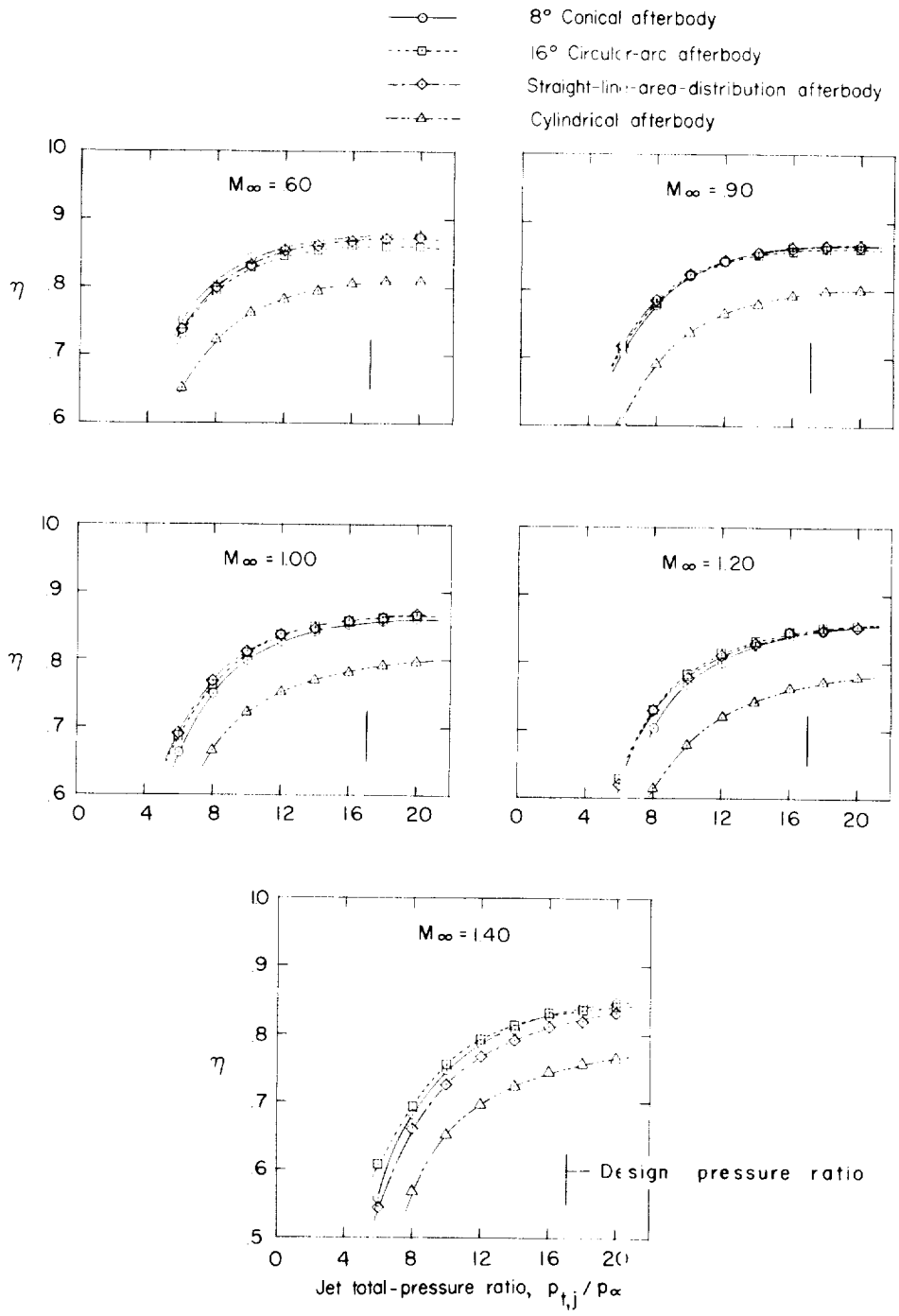

(d) Nozzle length of 3.52 inches.

Figure 8.- Concluded

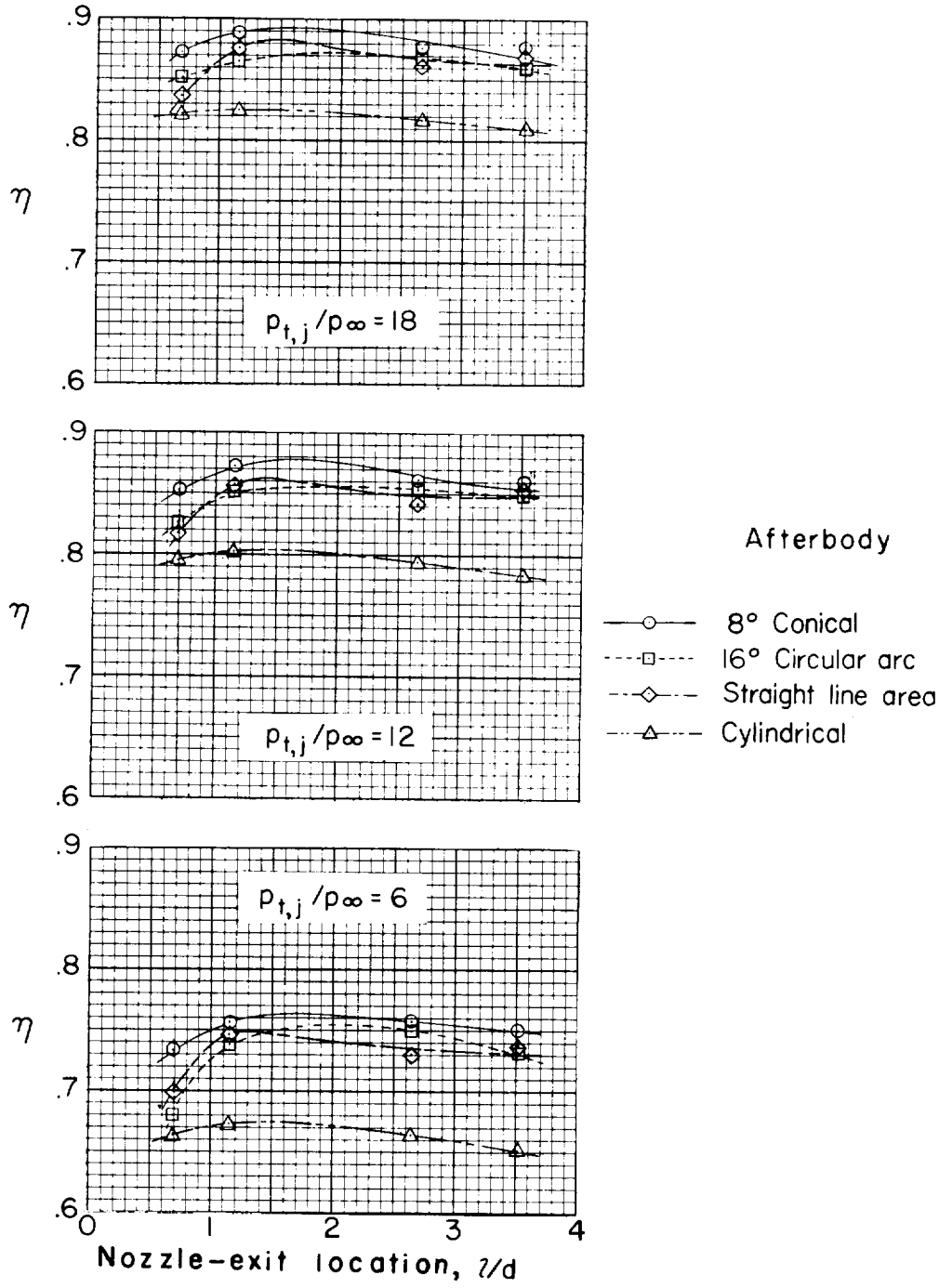

(a) $M_\infty = 0.60$.

Figure 9.- Effect of nozzle length on the efficiency factor.

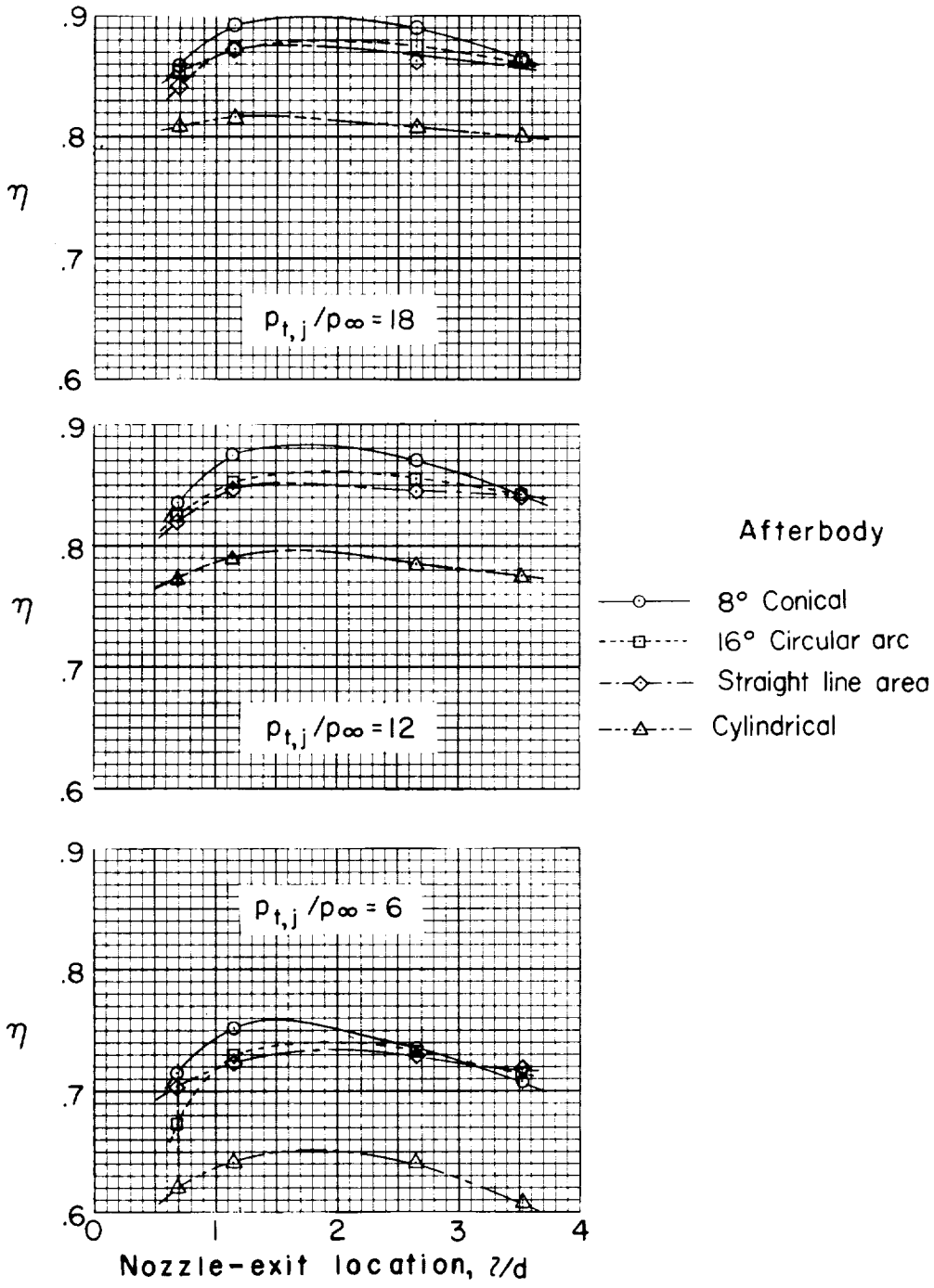

(b) $M_\infty = 0.90$.

Figure 9.- Continued.

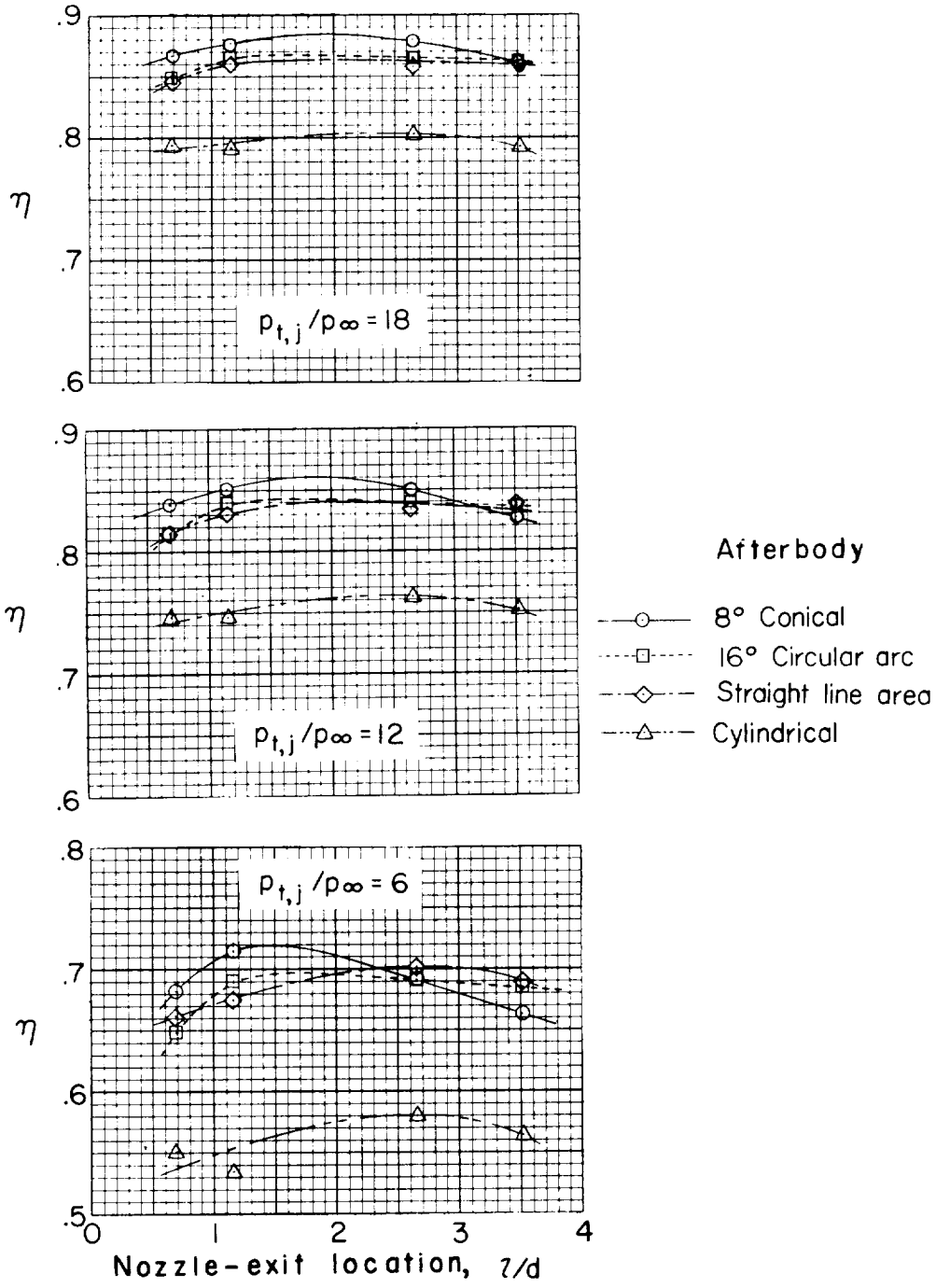

(c) $M_\infty = 1.00$.

Figure 9.- Continued.

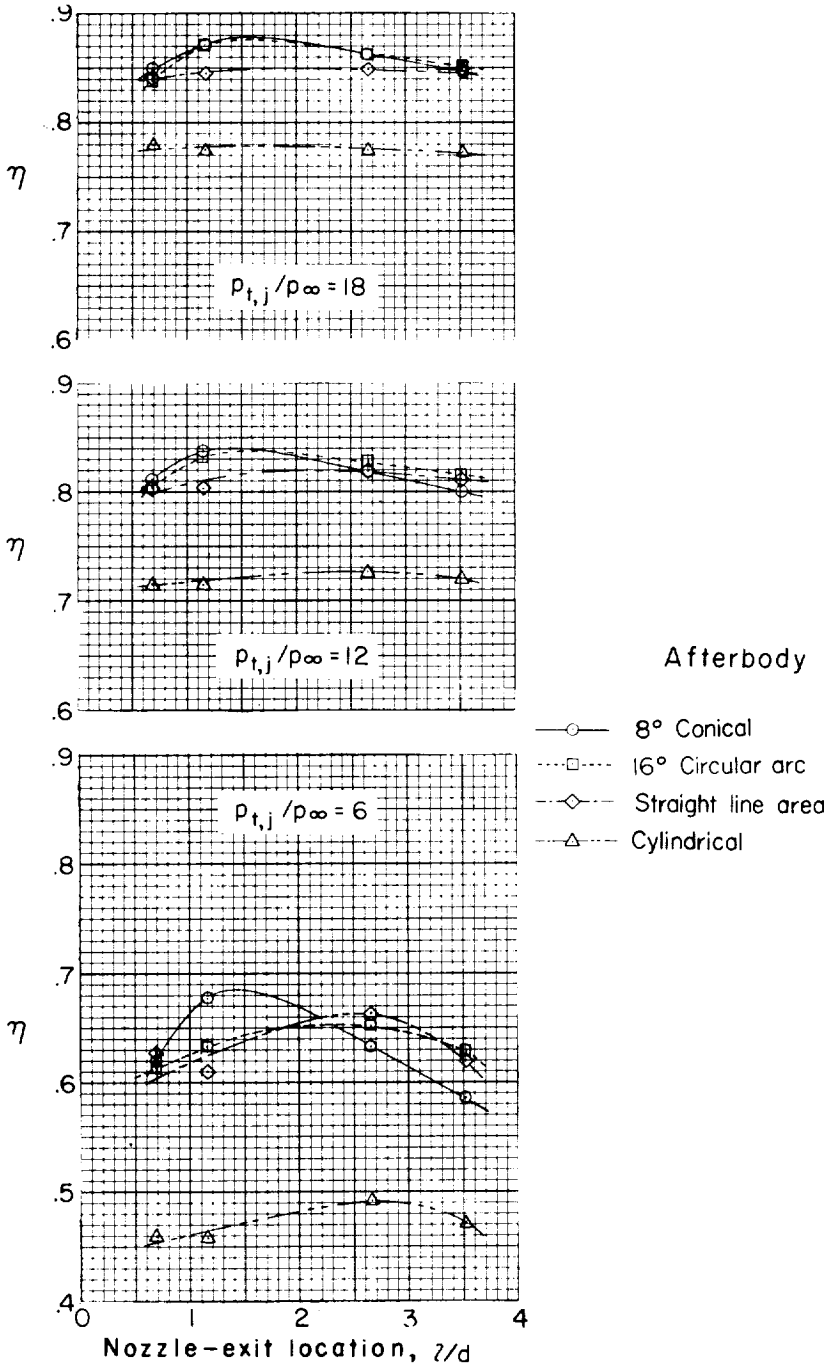

(d) $M_\infty = 1.20$.

Figure 9.- Continued.

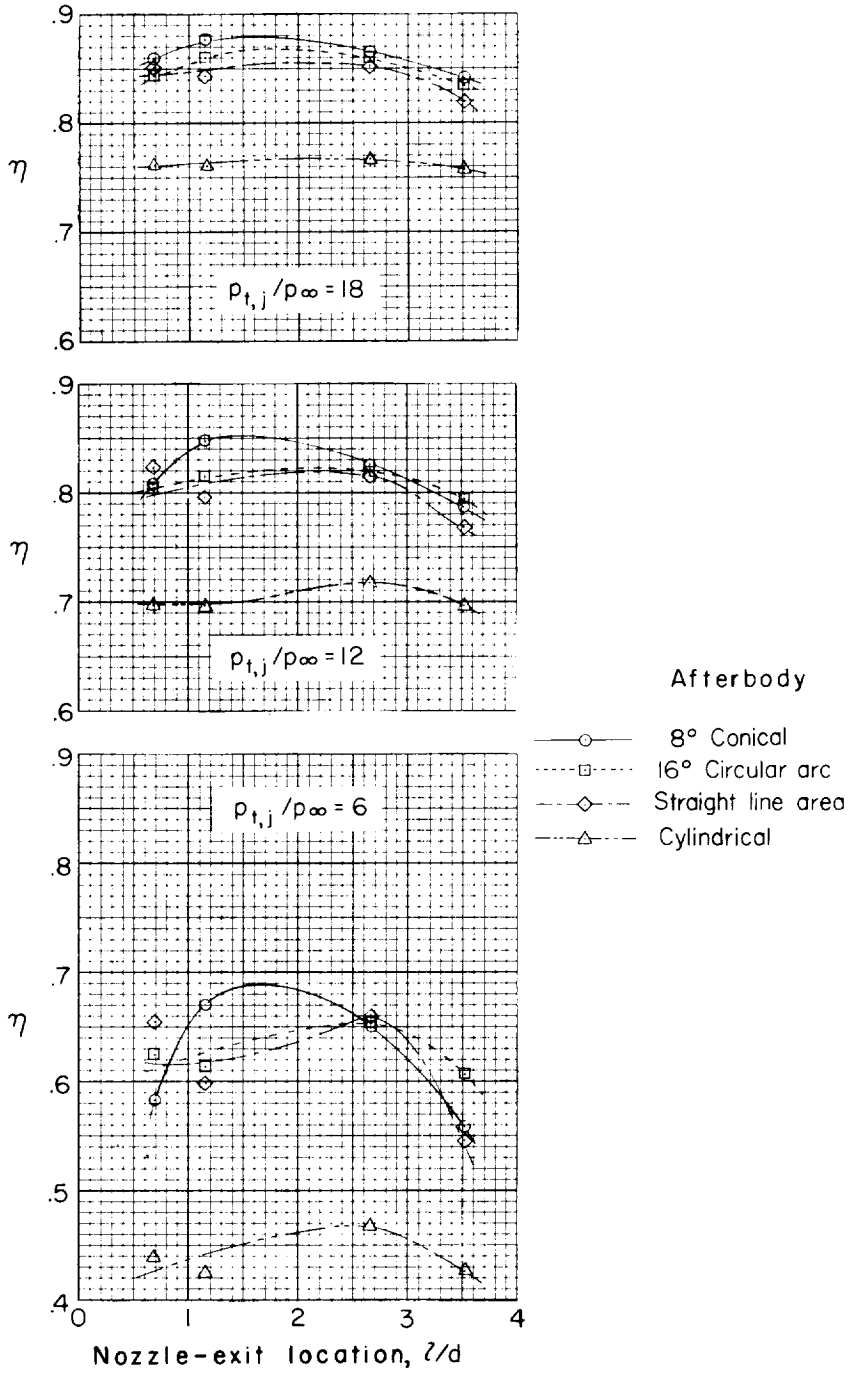

(e) $M_\infty = 1.40$.

Figure 9.- Concluded.

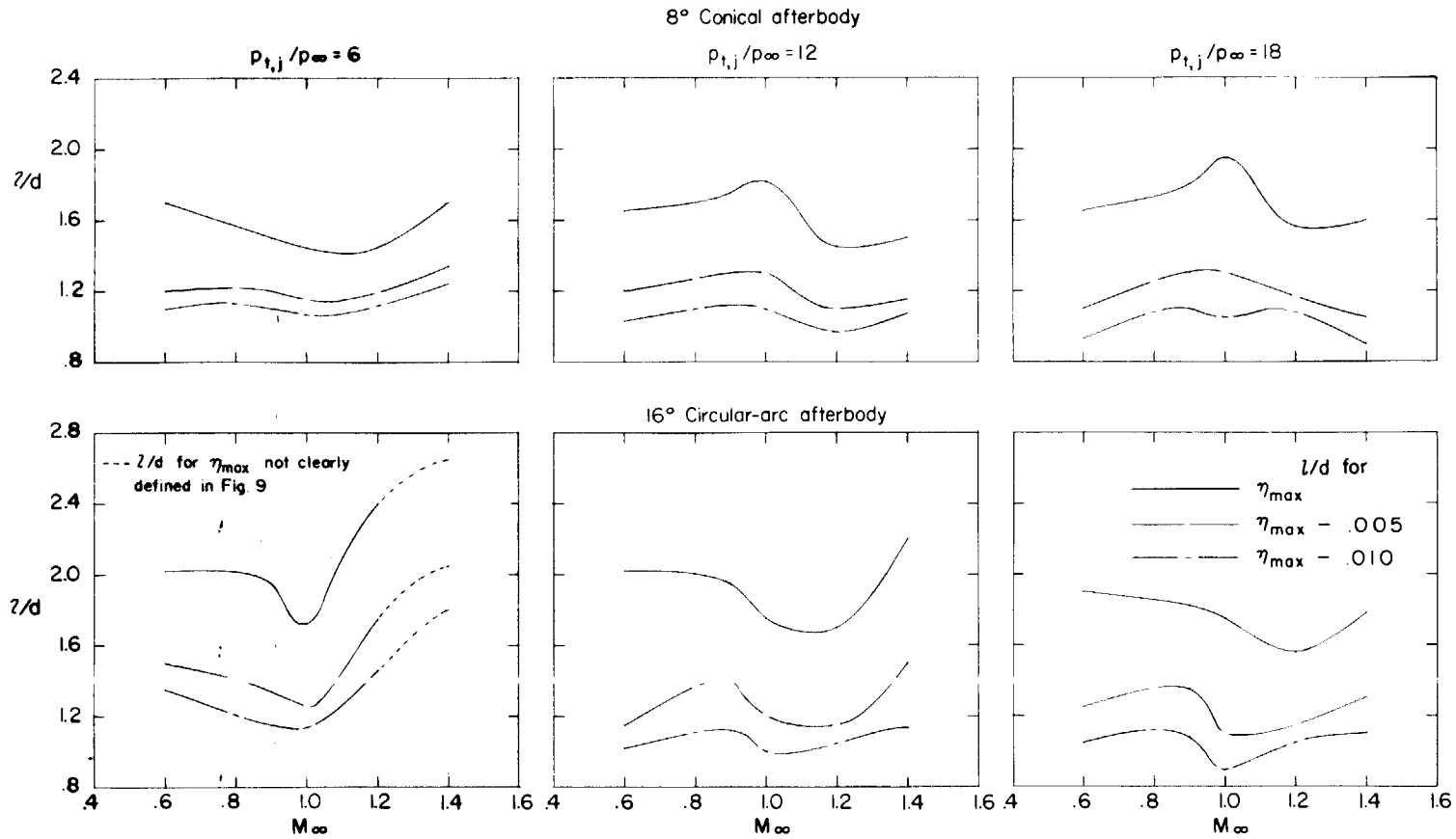

(a) 8° cone and 16° circular-arc afterbodies.

Figure 10.- Effect of Mach number on the nozzle extension factor.

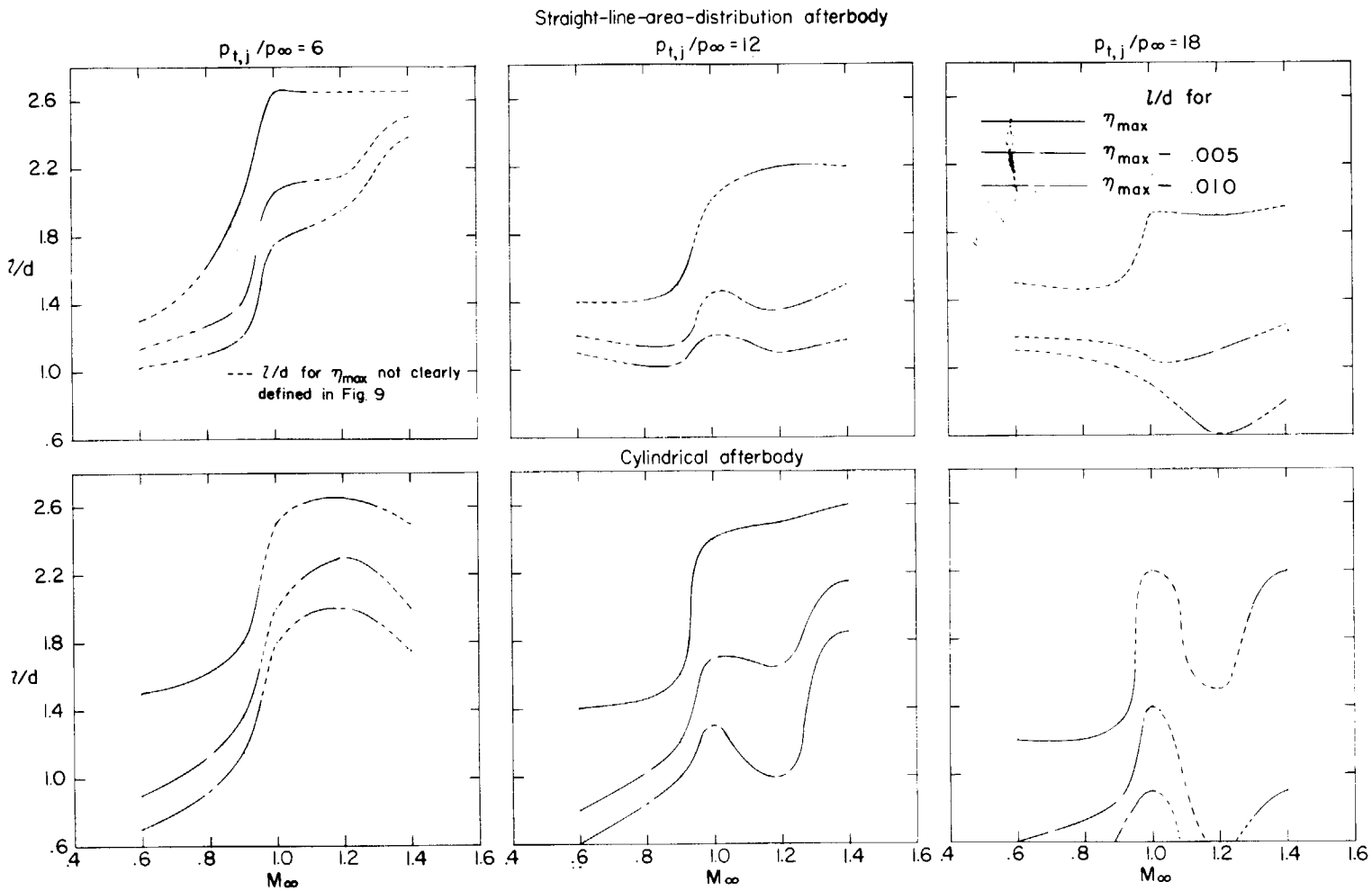

(b) Straight-line-area-distribution and cylindrical afterbodies.

Figure 10.- Concluded.

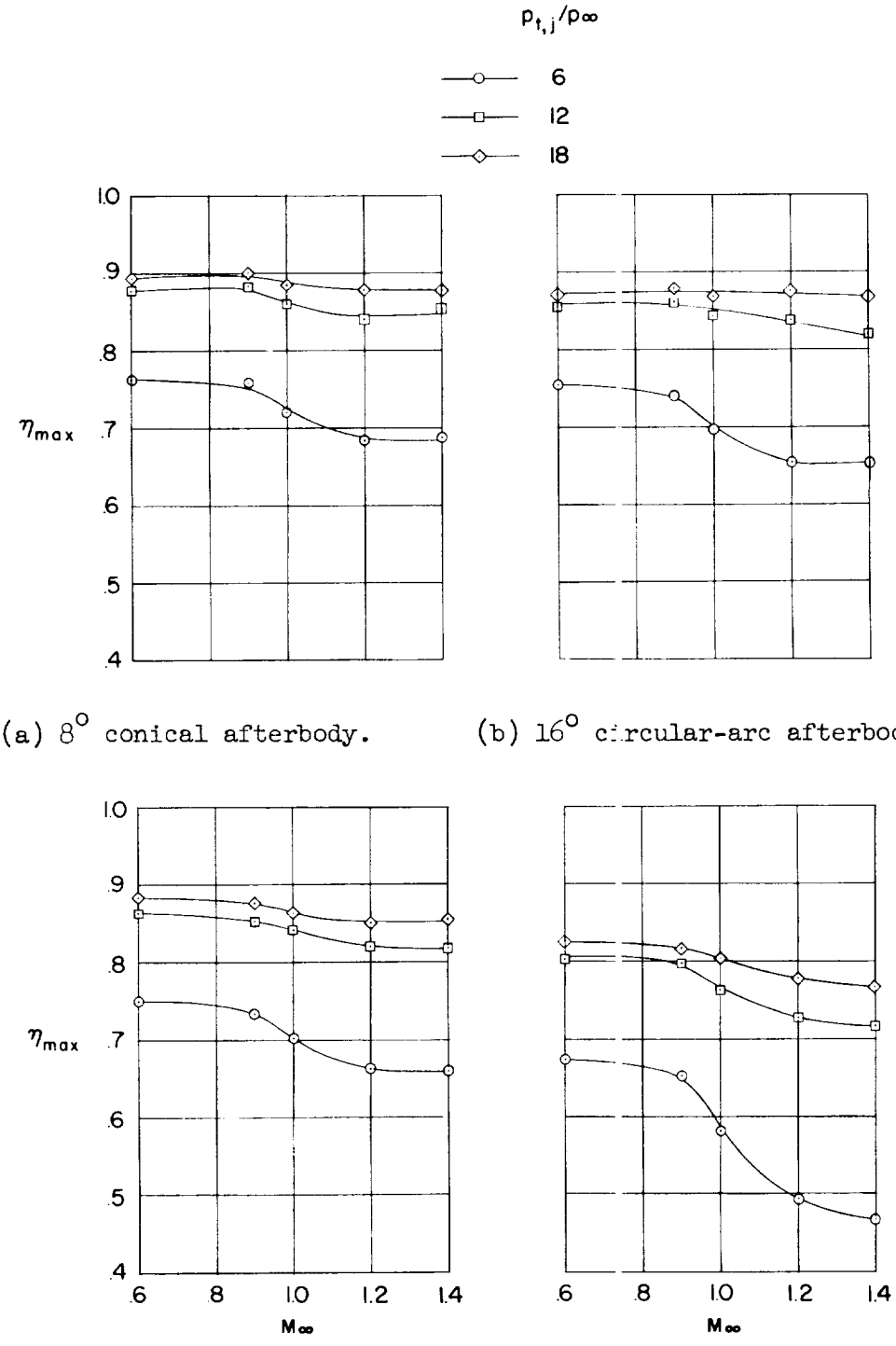

(a) 8° conical afterbody.

(b) 16° circular-arc afterbody.

(c) Straight-line-area-distribution afterbody.

(d) Cylindrical afterbody.

Figure 11.- The effect of Mach number on the maximum efficiency factor.

NASA - Langley Field, Va. L-862

L-862